Neutrons in Radiotherapy: Semiconductor Dosimetry

Anatoly Rozenfeld

CENTRE FOR MEDICAL RADIATION PHYSICS
UNIVERSITY OF WOLLONGONG

Prague, 23-27 June , 2015

Summary

Principle of Semiconductor Neutron Dosimetry in:

- Fast Neutron Therapy
- Boron Neutron Capture Therapy
- Proton Therapy
- Medical X-ray LINAC

Physics of Neutron Therapy

- Indirectly ionizing
- Sets in motion protons and heavy recoils

Elastic: n + X → n + X

Inelastic: n + X → C* → b + Y

(n,n) (n,p) (n,d) (n,α) (n,γ) (n, X)

- Neutrons deposit 20-100 times more energy per unit length than x-rays (LET: 100eV/μ)
- Neutrons always accompanied by gamma radiation:

$$D_{Total} = D_{neutron} + D_{\gamma}$$

Physics of Neutron Therapy

- Total dose can be measured with ion chambers based on Bragg-Gray relationship:

$$D_T = \frac{Q_n}{m} \cdot \frac{W_n}{e} \cdot \left(r_{m,g}\right)_n \cdot \left(\frac{K_t}{K_m}\right) \cdot d_T \cdot \frac{1}{1+\delta}$$

Physics of Neutron Therapy

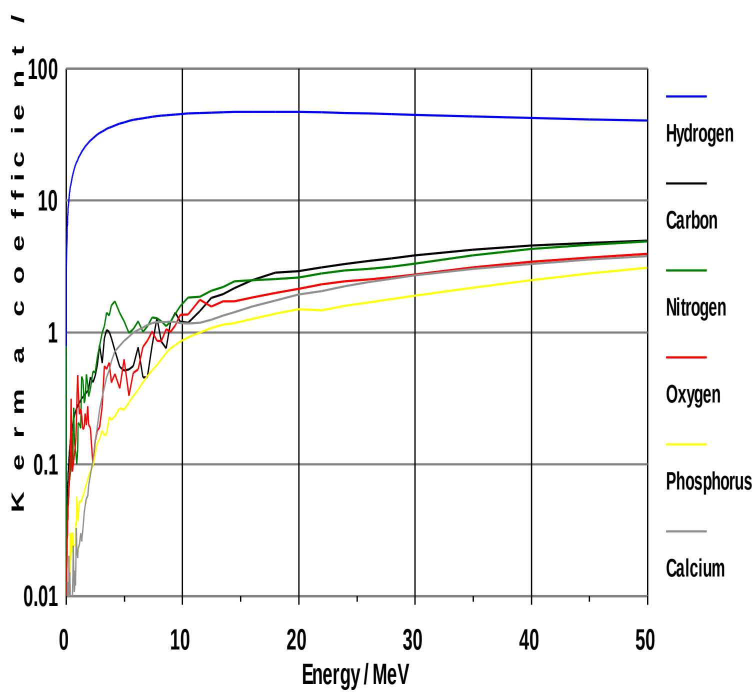

- Effect of tissue elemental composition on neutron dosimetry

Tissue	Kerma
Muscle	5.85 fGy·m^2
Inner Bone	5.28 "
Cortical Bone	3.05 "
Adipose	6.57 "
Lung	5.88 "

CENTRE FOR MEDICAL RADIATION PHYSICS
UNIVERSITY OF WOLLONGONG

Radiobiology of Neutron Therapy

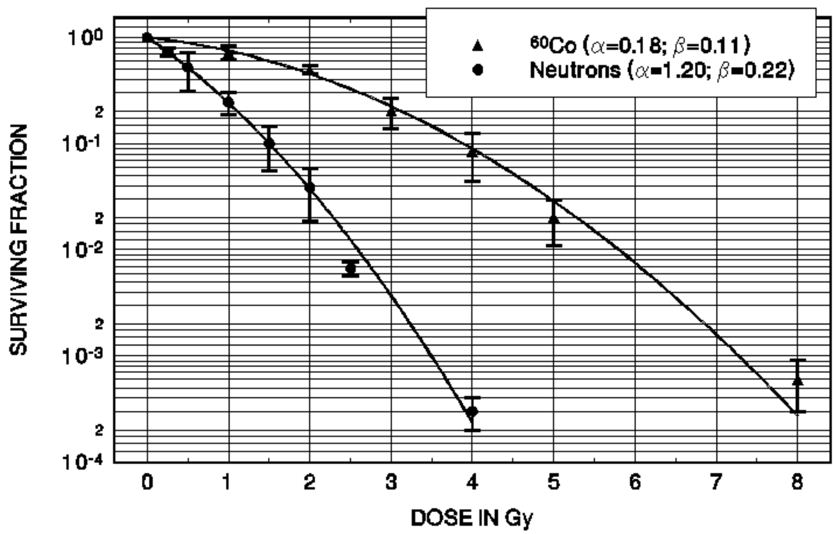

- Steep survival curves
- Low OER
- Less variability in radio-sensitivity across the cell cycle

Radiobiology of Neutron Therapy

- Less repair of sublethal and potentially lethal damage
- Hypoxic and slowly growing tumors
- Increased RBE
  - RBE=4 for cancer
  - RBE=3 for normal tissue

Harper Hospital Superconducting Cyclotron: Operational Parameters

- Liquid He: 100 liters
- Magnetic Field: from 4.6T to 5.4T
- RF: 105 MHz from 25kW transmitter
- Magnet Current: 203 A
- Ion Source: deuterium discharge (2.8 kV, 350mA)
- Target: Be (15.9 x 20.1 x 3.2 mm), 20.3^{o}
- Beam Current: 15 μA
- Neutron Production: d(48.5)+Be

Harper Hospital Superconducting Cyclotron: Operational Parameters

- Cyclotron: 25 T
- Beam Stop: 25 T
- Mounted on two concentric rings
- Full 360º rotation
- Isocenter: 1829 mm
- Output: 3.2 $cGy \cdot min^{-1} \cdot \mu A^{-1}$

Harper Hospital Superconducting Cyclotron: Installation

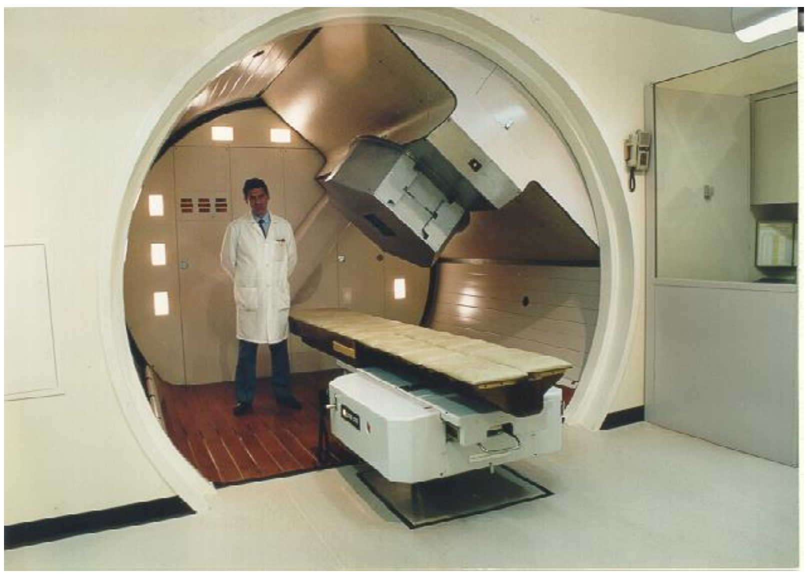

- 1990 - Under direction of Prof . Richard. L. Maughan
- Sept. 1991: First patient treated
- March 1992: Clinical trials

Multi-Rod Collimator

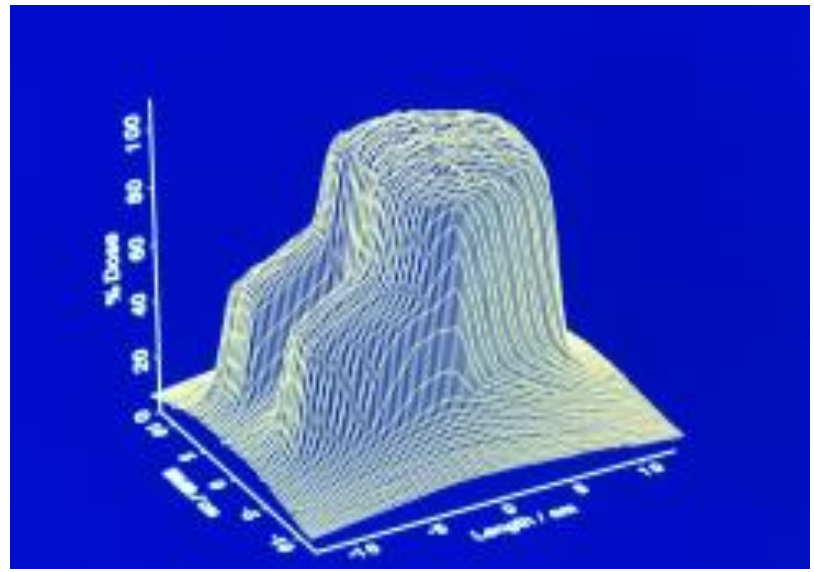

Neutron Beam Physical Characteristics: Depth Dose

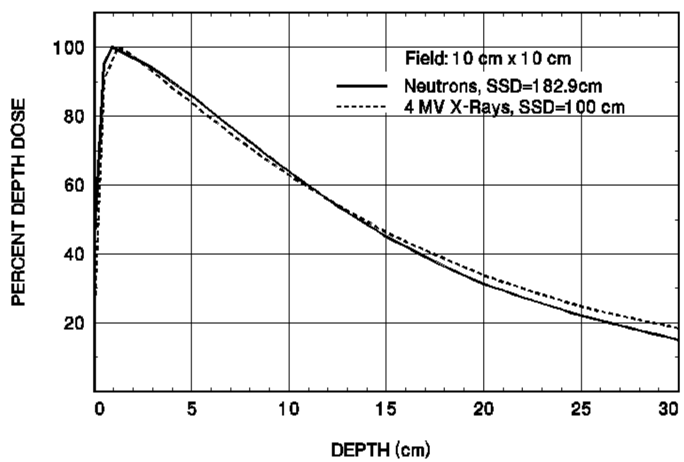

- Resembles 4 MV Photons
- d_{max} = 0.9 cm in tissue
- $d_{50\%}$ = 13.6 cm
- $D_{surface}$ = 42%
- Penumbra (20%-80%):
  0.60 cm @ d_{max}
  1.90 cm @ 10 cm depth
  3.40 cm @ 20 cm depth

TOTAL DOSE EFFECTS on MOSFETs: Voltage threshold shifting

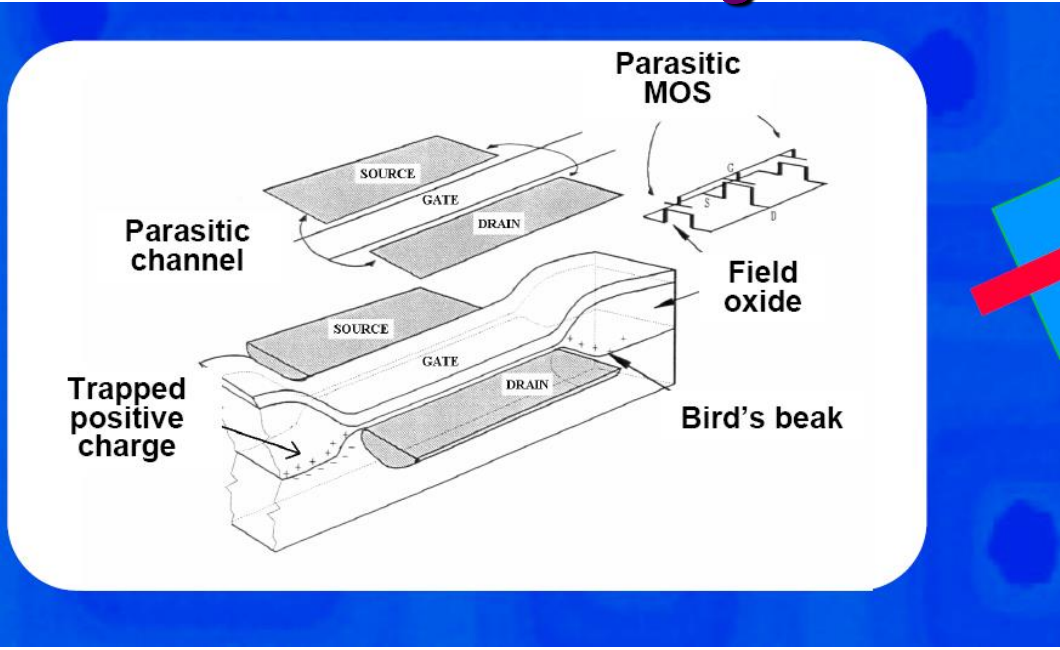

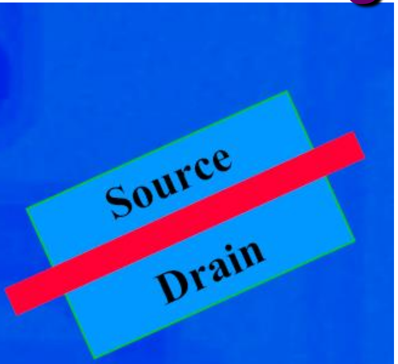

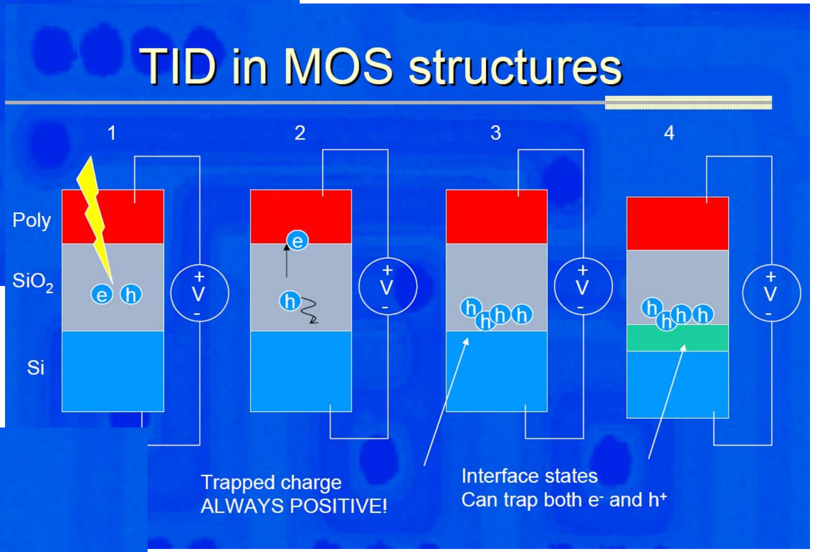

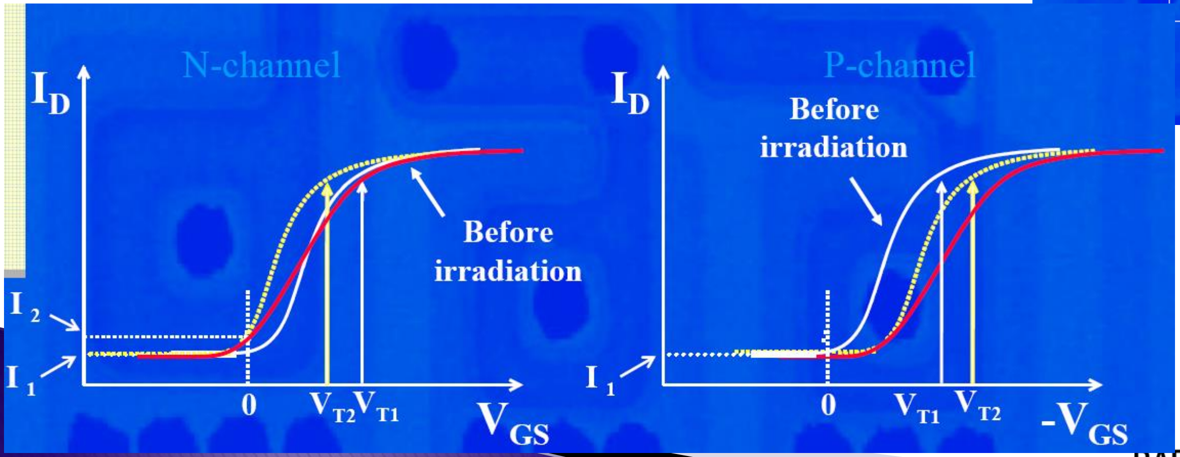

CENTRE FOR MEDICAL RADIATION PHYSICS
UNIVERSITY OF WOLLONGONG

Radiation damage in silicon detectors: The microscopic point of view

- Radiation induced lattice defects:
  - Traps
  - Generation and recombination centers
  - Clusters

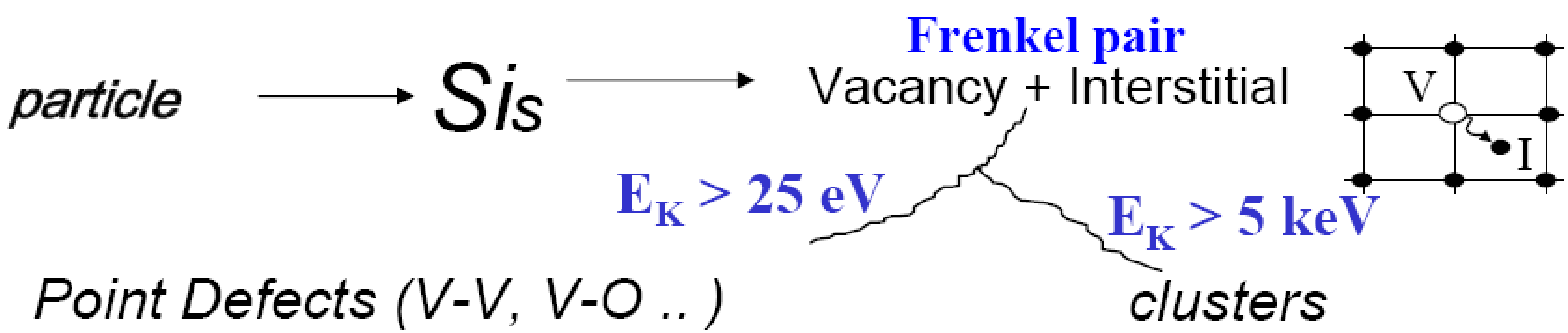

The microscopic point of view

Vacancy amount and distribution depends on particle kind and energy.

- ^{60}Co – gammas: Compton electrons → trapped charge (TID)
- Electrons:
  - low energy → displacement
  - High energy → clusters
- Neutrons:
  - Thermal → displacement
  - Fast → clusters

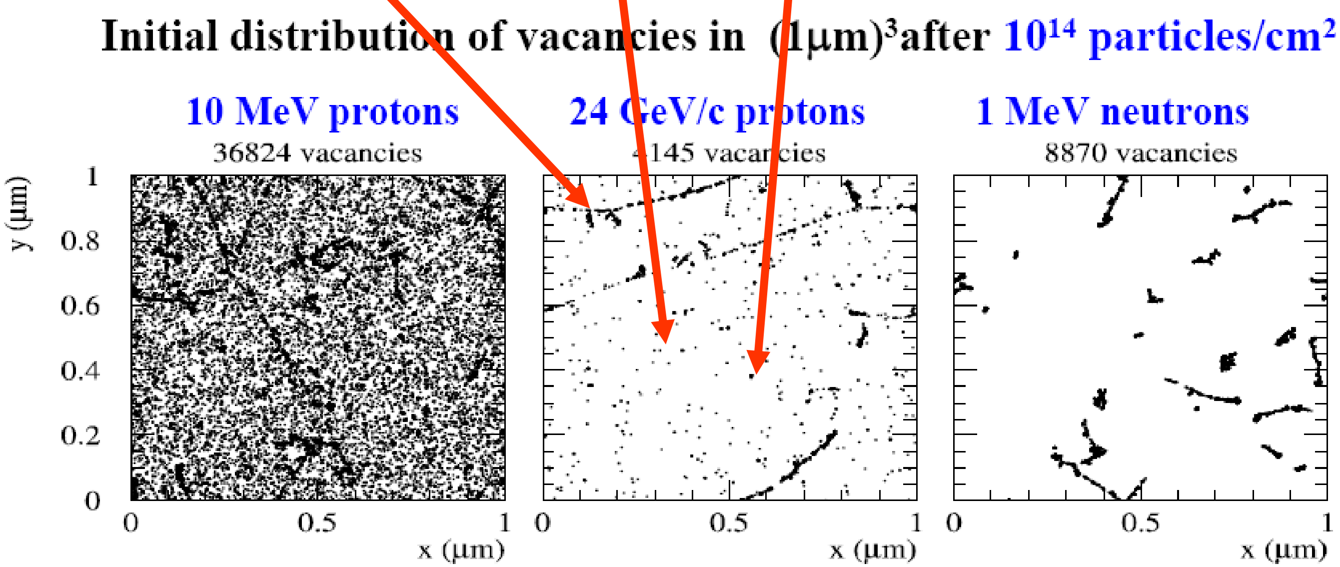

[Mika Huhtinen NIMA 491(2002) 194]

The microscopic point of view

Primary Damage and secondary defect formation

- **Two basic defects**

  I - Silicon Interstitial   V - Vacancy

- **Primary defect generation**

  I, I_2 higher order I (?)

  $\Rightarrow$ **I** - CLUSTER **(?)** $\Longleftarrow$

  V, V_2, higher order V (?) **Damage?!**

  $\Rightarrow$ **V** - CLUSTER **(?)** $\Longleftarrow$

- **Secondary defect generation**

  Dopants : P, B

  Main impurities in silicon: Carbon C_s

  Oxygen O_i

  Oxygen dimer: O_{2i}

$I+C_s \rightarrow C_i \Rightarrow$

$C_i+C_s \rightarrow C_iC_s$

$C_i+O_i \rightarrow C_iO_i$

$C_i+P_s \rightarrow C_iP_s$

$I + O_{2i} \rightarrow IO_{2i}$

$V+V \rightarrow V_2$ $V+V_2 \rightarrow V_3$

$V+O_i \rightarrow VO_i \Rightarrow$ $V+VO_i \rightarrow \underline{V_2O_i}$

$V+P_s \rightarrow VP_s$

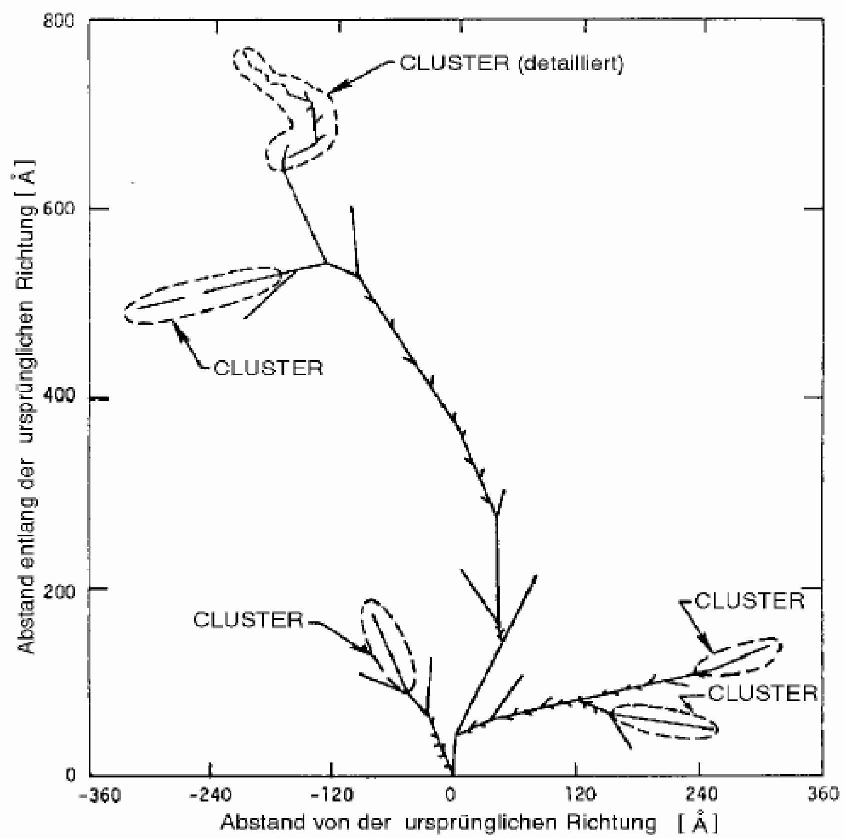

The microscopic point of view

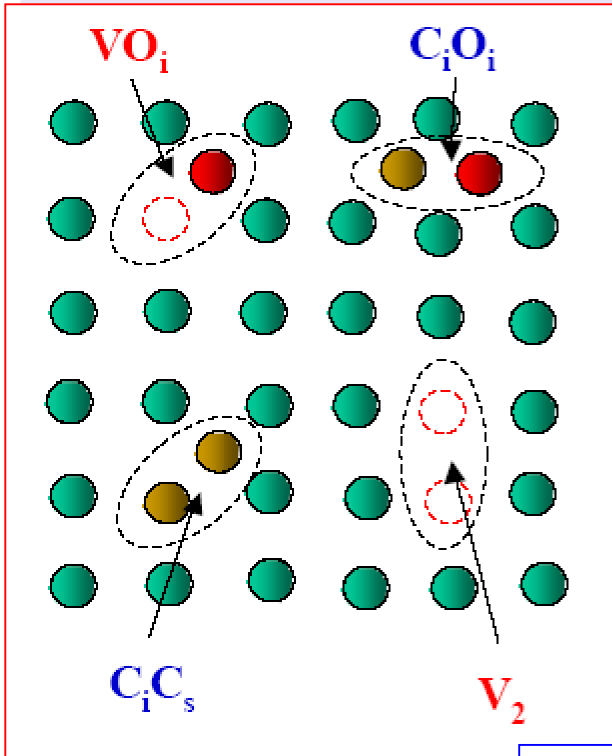

Quasi-chemistry

with complex kinetics (time, concentration, temperature dependences)

O = Oxygen
C = Carbon
P = Phosphorus
I = interstitial
S = substitutive
V = vacancy

Various quasi-chemical reactions

$V+V \rightarrow V_2$ $\quad$ $V+V_2 \rightarrow V_3$

$V+O_i \rightarrow VO_i \Rightarrow$ $\quad$ $V+VO_i \rightarrow V_2O_i$ $\quad$ $V+V_2O_i \rightarrow V_3O_i$

$V+P_s \rightarrow VP_s$

$I+VP_s \rightarrow P_s$ $\quad$ $I+V_2 \rightarrow V$

$I+VO_i \rightarrow O_i$ $\quad$ $I+V_2O_i \rightarrow VO_i$ $\quad$ $I+V_3O_i \rightarrow V_2O_i$

$I+C_s \rightarrow C_i \Rightarrow$ $\quad$ $C_i+C_s \rightarrow C_iC_S$

$C_i+O_i \rightarrow C_iO_i$

The microscopic point of view

- Energy Levels related to traps: **main parameters**
  - E_t: Activation energy
  - σ: Cross section
  - N_t: Concentration

Emission coefficient:

$$e_n = N_c \sigma_n v_{th} \cdot e^{-\frac{E_c - E_t}{KT}}$$

Capture coefficient :

$$c_n = n \sigma_n v_{th}$$

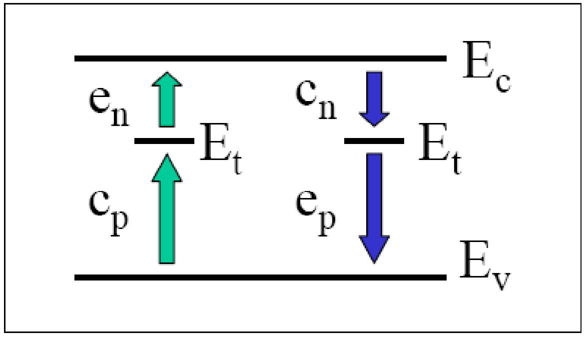

From microscopic to MACROSCOPIC point of view

Impact of Defects on Detector properties

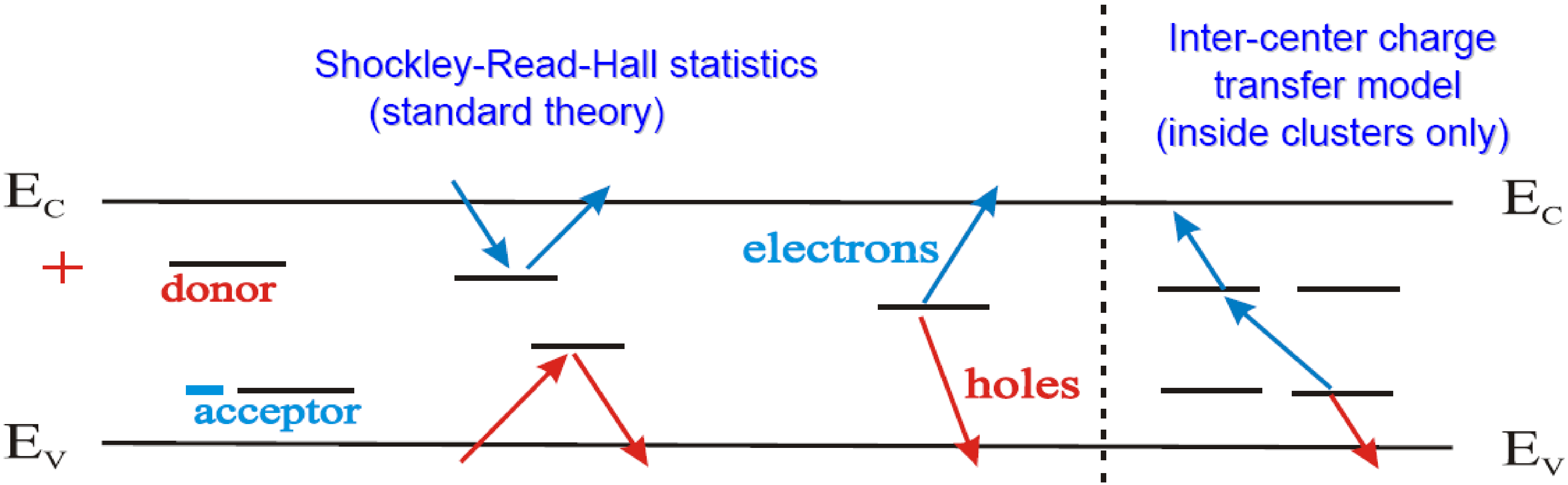

charged defects
⇒ **N_{eff} , V_{dep}**
e.g. donors in upper and acceptors in lower half of band gap

Trapping (e and h)
⇒ **CCE**
shallow defects do not contribute at room temperature due to fast detrapping

generation
⇒ **leakage current**
Levels close to midgap most effective

enhanced generation
⇒ **leakage current**
⇒ **space charge**

Impact on detector properties can be calculated if all defect parameters are known:

$\sigma_{n,p}$: cross sections **ΔE : ionization energy** **N_t : concentration**

The MACROSCOPIC point of view

- Leakage current:

$$\frac{I_{dep}}{Volume} = \alpha \cdot \Phi$$

$$\alpha = 4 \cdot 10^{-17}\ A/cm$$

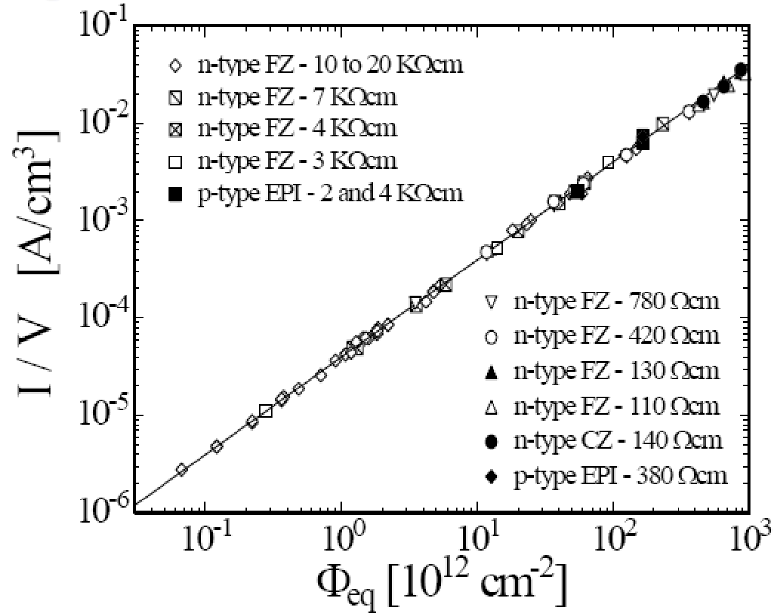

- Variation of doping concentration:

$$\Delta N_{eff}(\Phi) = \left| N_{C0}(1 - e^{-c\Phi}) - \beta \cdot \Phi \right|$$

Compensation of shallow doping concentration

Acceptor defects production

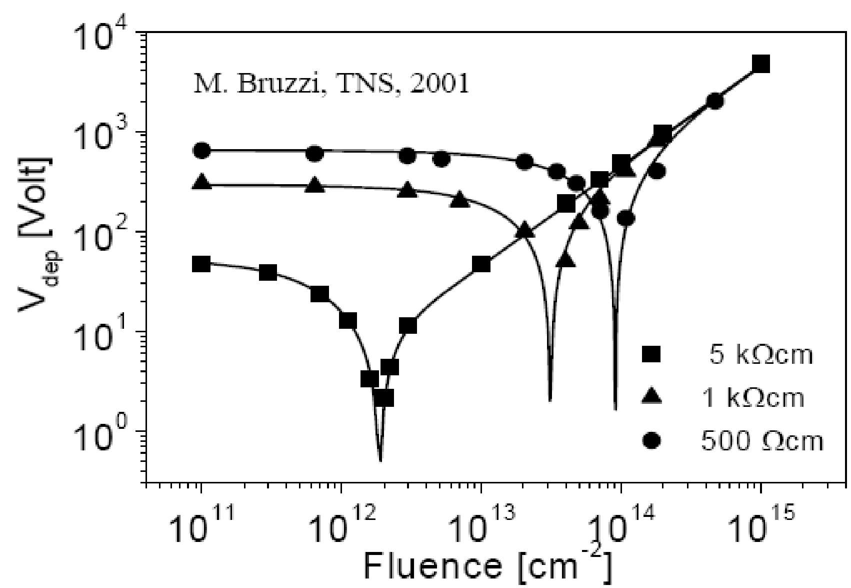

The MACROSCOPIC point of view

- Decreasing of Charge Collection Efficiency (CCE):

$$Q = Q_o \cdot \varepsilon_{dep} \cdot \varepsilon_{trap}$$

Where Q=collected charge
Q_0=pre-irradiation collected charge
ε_{dep}= sensitive volume "efficiency"
ε_{trap}= collection time "efficiency"

$$\varepsilon_{dep} = \frac{W_0}{W_D} \qquad \varepsilon_{trap} = e^{-\frac{\tau_c}{\tau_t}} \qquad W_D = W_0 + L = \sqrt{\frac{2\varepsilon \cdot V_{bi}}{q \cdot N_{eff}}} + \sqrt{D_h \cdot \tau_h}$$

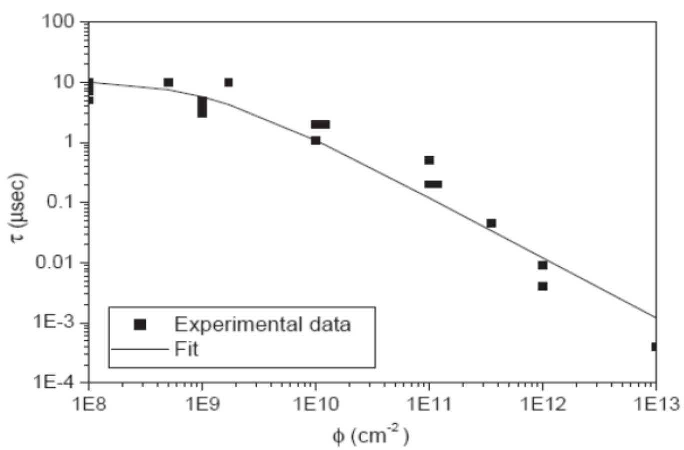

$$\frac{1}{\tau} = \frac{1}{\tau_0} + k_\tau \phi,$$

Per protoni da 10MeV

$$k_\tau = (1.52 \pm 0.05) \times 10^{-11}\ \mu s^{-1}\ cm^2$$

The MACROSCOPIC point of view

Dosimeters for radiation therapy – from 1983 to 2010!!

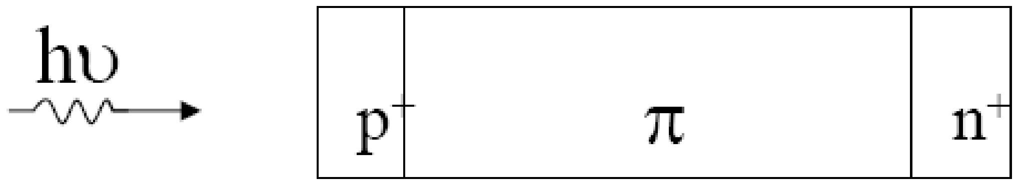

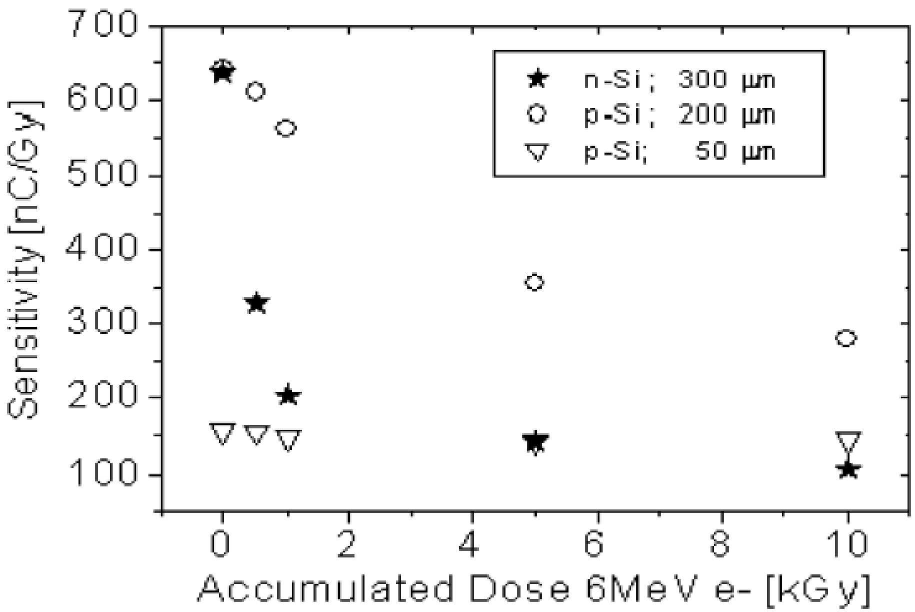

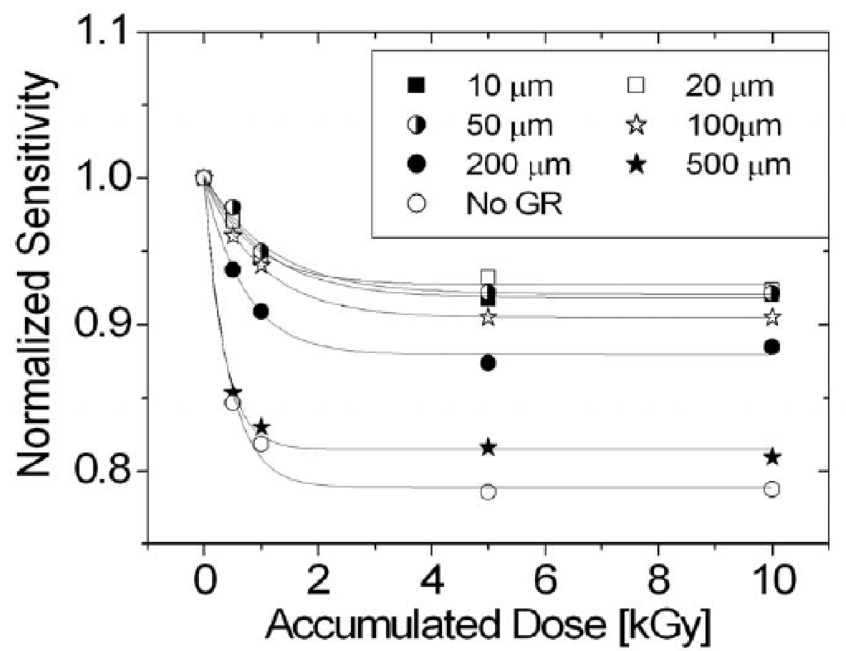

M. Bruzzi et al. App. Phys. Lett, 2007.

Tissue and Silicon Neutron Kerma

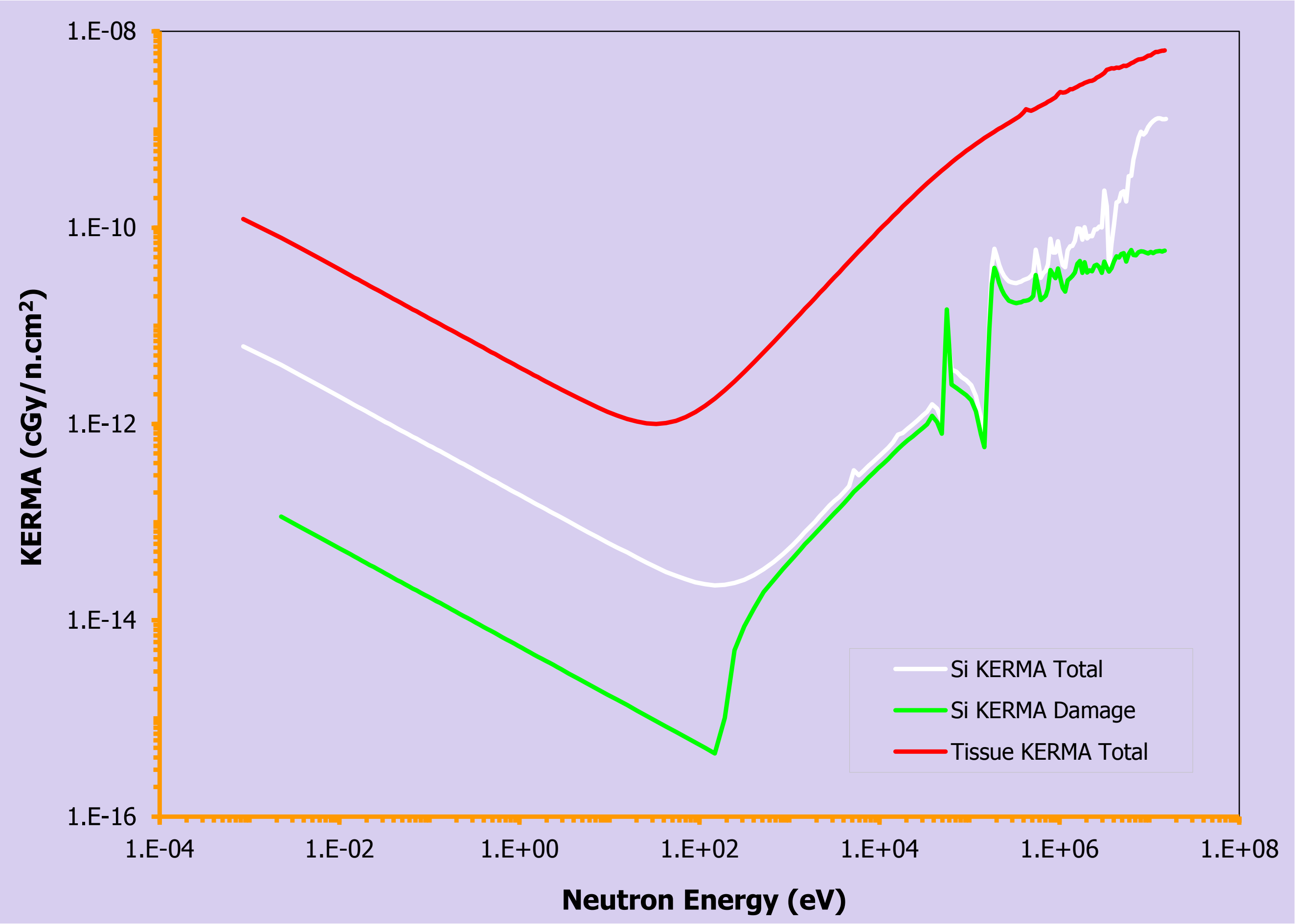

Ratio of Si Displacement Kerma to Tissue Kerma for Neutrons

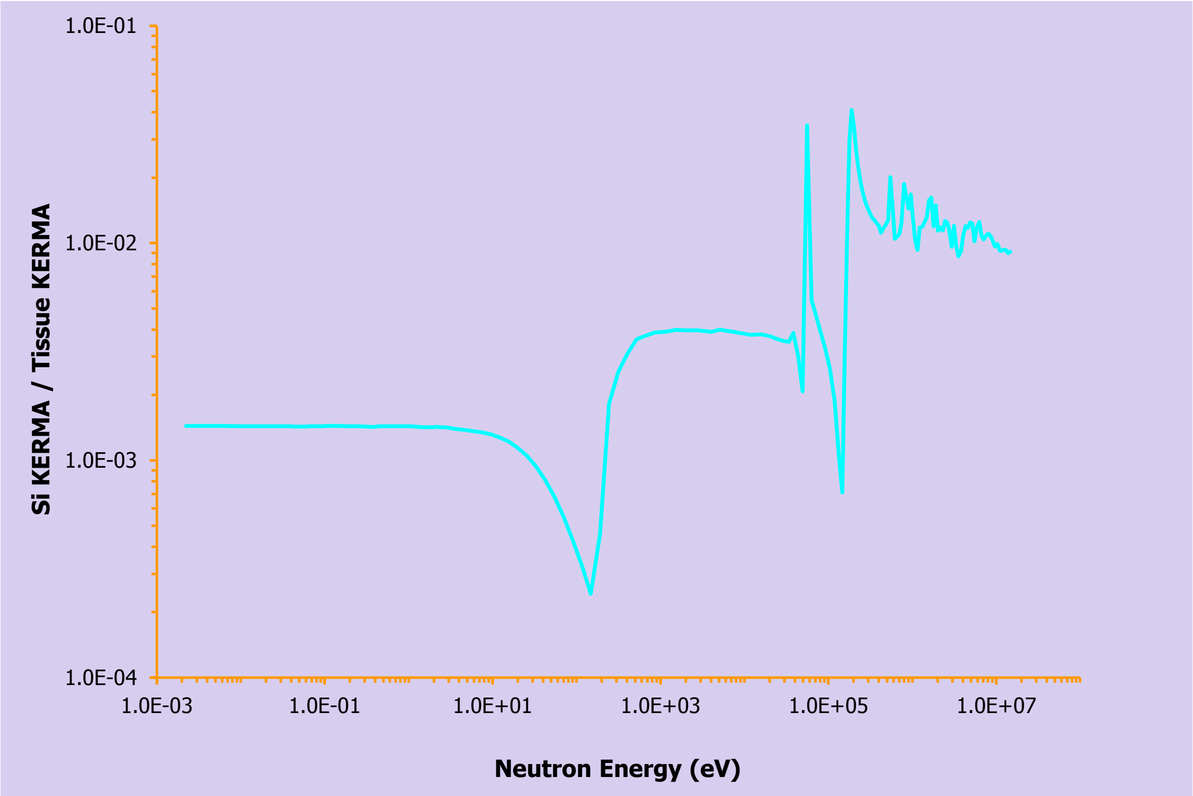

The ratio of Si displacement KERMA to tissue KERMA over some energy intervals is almost energy independent

Method of neutron dosimetry

- The operation of the *p-i-n* diode neutron sensor is based on the change of forward voltage

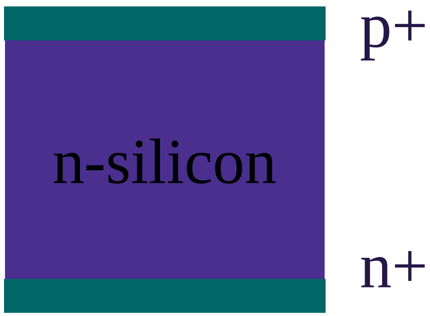

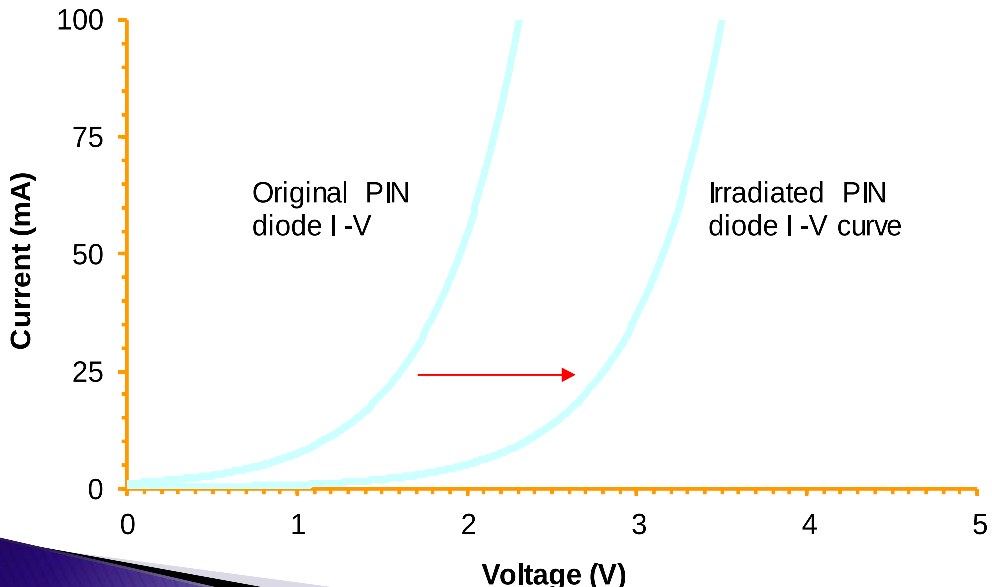

$$\frac{1}{\tau} - \frac{1}{\tau_0} = k_\tau \Phi$$

Sensitivity =αW^2

W-diode base length

Bulk and Planar Neutron Diodes

Neutron detectors based on radiation damage

D-Type

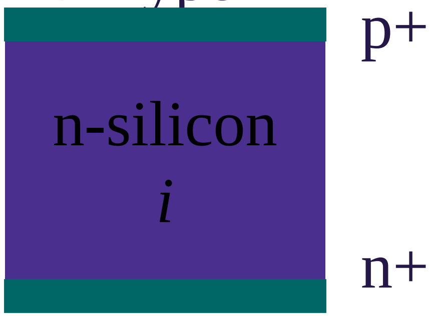

L-Type

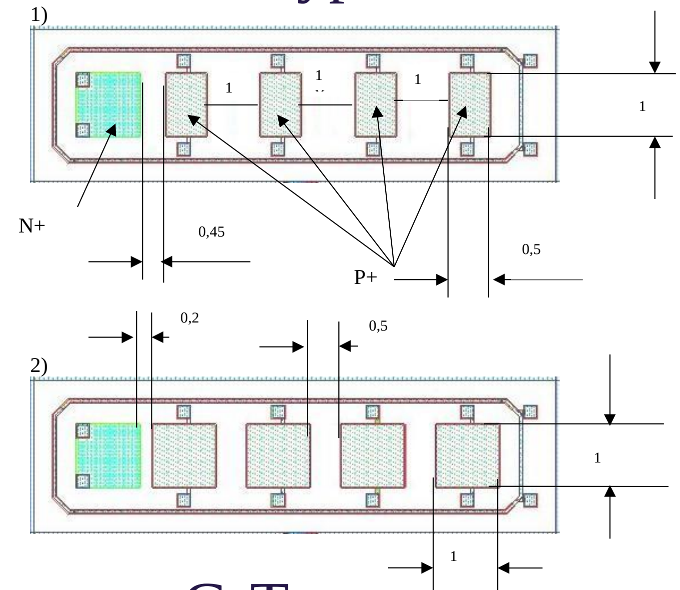

C-Type

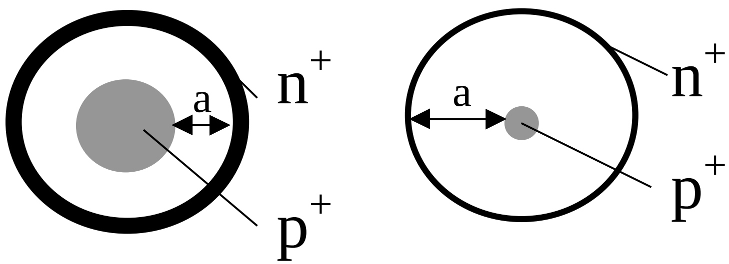

C - 1   C - 2

G-Type

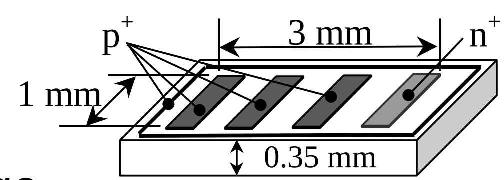

Passive sensor: based on forward voltage change after irradiation

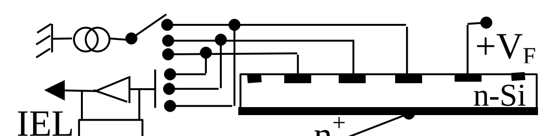

Introduction

- New type of semiconductor dosimeters based on ion implanted miniature planar *p-i-n* diodes was developed
- Dosimeter combines two types:
  - Planar p-i-n diodes
  - Bulk p-i-n diodes
- The forward voltage drop across the p-i-n diode is proportional to neutron induced damage (NIEL) and correlates with neutron dose
- The current produced due to the secondary charged particle interactions (IEL) correlates with the total (neutron + gamma) dose

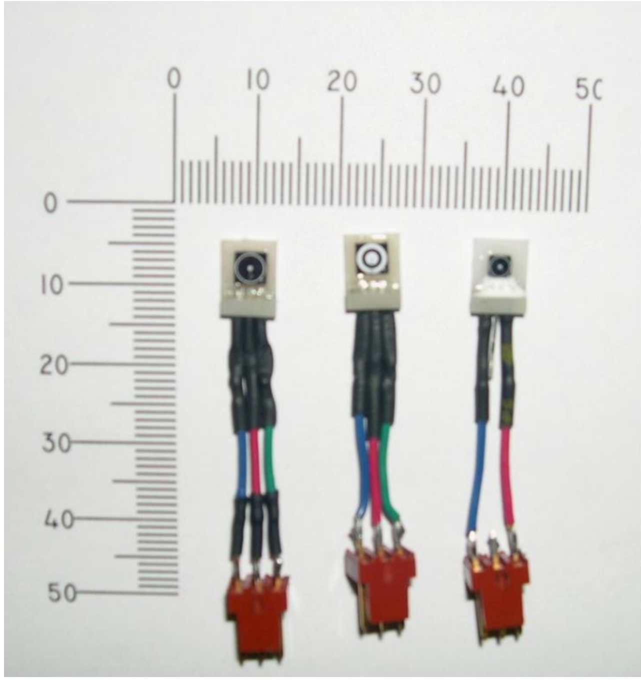

Application for Neutron Dosimetry

- The response of the diode in mixed ($D_n + D_\gamma$) beam:
  - Voltage drop mode:

$$R_{mV} = C_{n,mV} \cdot D_n$$

  - Charge mode:

$$R_{nC} = C_{n,nC} \cdot D_n + C_\gamma \cdot D_\gamma$$

$C_{n,mV}$ is the sensitivity of the diode to neutrons in mV/cGy

$C_{n,nC}$ is the sensitivity of the diode to neutrons in nC/cGy

C_γ is the sensitivity of the diode to gamma in nC/cGy

Fast Neutron Therapy

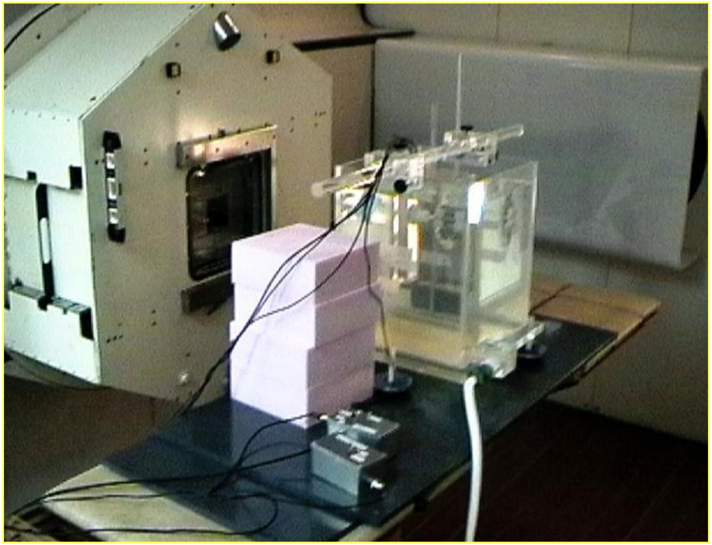

Gershenson Radiation Oncology Center, Harper Hospital, Detroit

Phantom depth 5cm in water,

10 x 10 cm^2 beam, central axis

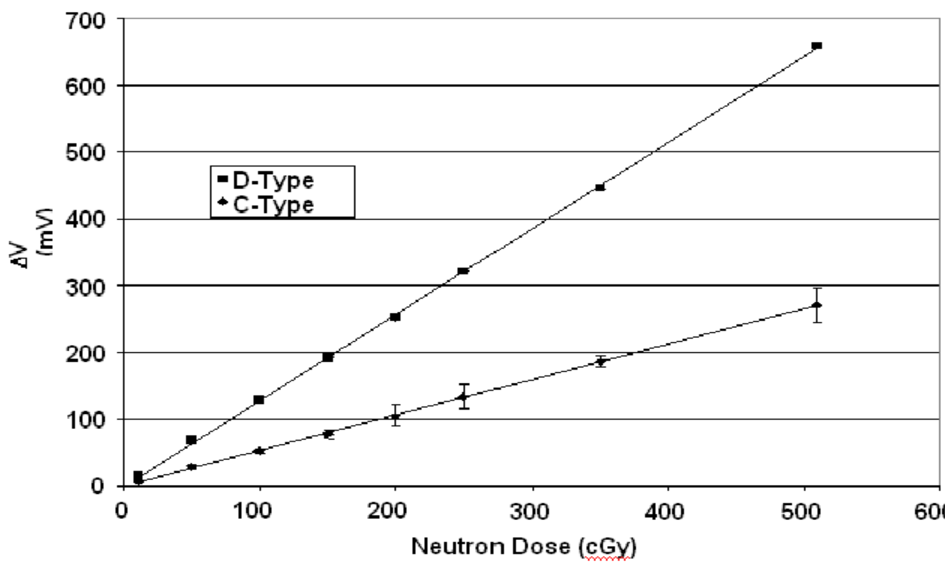

Two types of neutron *p-i-n* diodes were investigated –

D type bulk Si sensor $1mm^3$

C type planar circular shape

Neutron response of C-Type *p-i-n* diodes

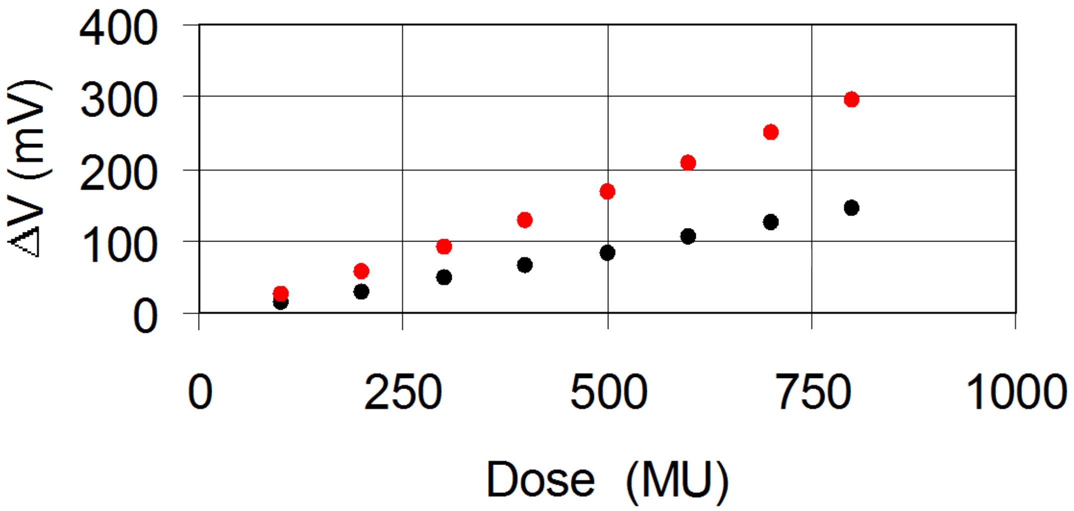

Neutron response of C-1 at depth 5 cm in a water for two readout currents 1 and 20 mA. The sensitivity is 0.14 mV/MU and 0.30mV/MU at point of irradiation.

Neutron response of C-2 at depth 5 cm in a water for two readout currents 1 and 20 mA. The sensitivity is 0.88 and 3.32 mV/MU for C-2 diode. 1 MU ~1cGy at point of irradiation

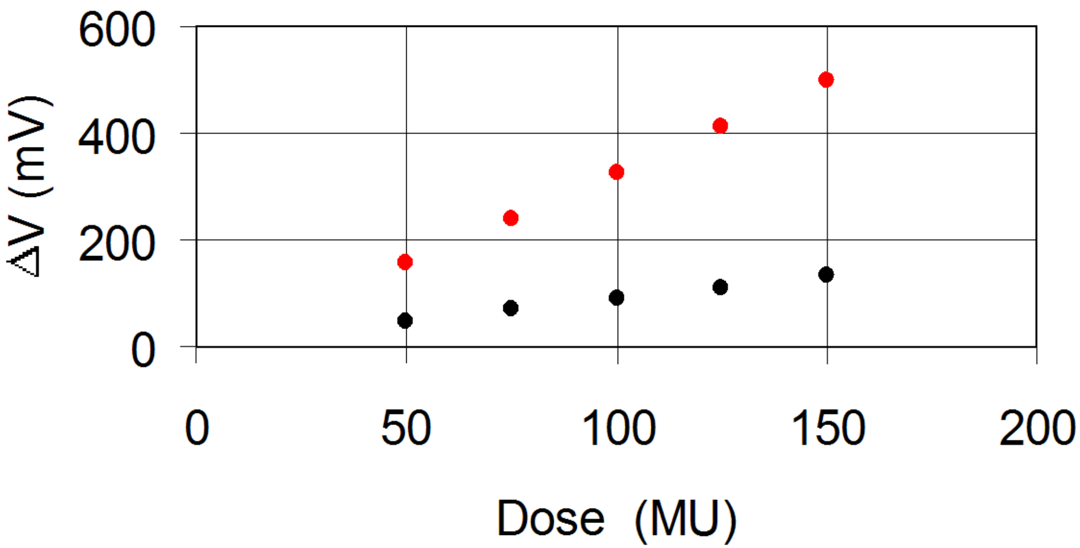

Beam Target Current and P-I-N Diode Voltage Drop

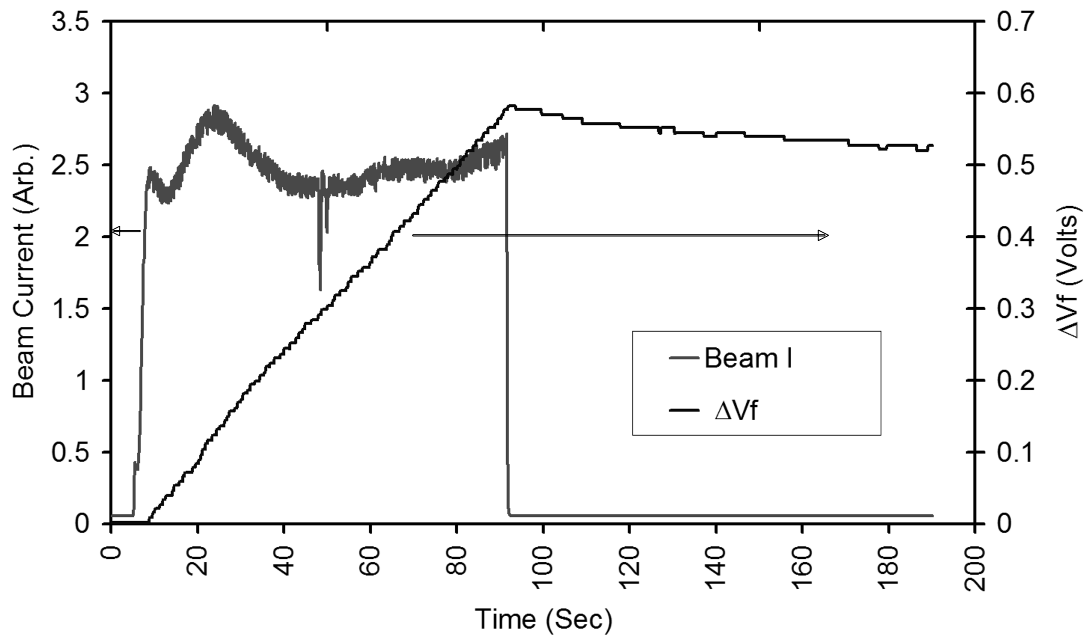

Neutron Production: d(48.5)+Be
d-beam current about 15uA

Objectives

- Determine the neutron and the gamma sensitivity of the diode for each mode of operation
- Investigate various dosimetry applications of the diode in *d(48.5)+Be* beam
  - Lateral beam profile
  - Central axis depth dose
  - Opened and closed collimator
- Compare the results with conventional dosimetry methods

Irradiation conditions

- *d(48.5)+Be* beam from clinical superconducting cyclotron
- Diodes embedded in A150 TEP holder
- Measurements:
  - In 5 × 5 cm^2 field in air
  - Lateral dose profile at 5 cm depth in 10 × 10 cm^2 field in a water phantom
  - Depth dose along the central axis in 10 × 10 and 15 × 15 cm^2 fields and 30 × 30 cm^2 field partially blocked with an equivalent of 93.5 mm of tungsten

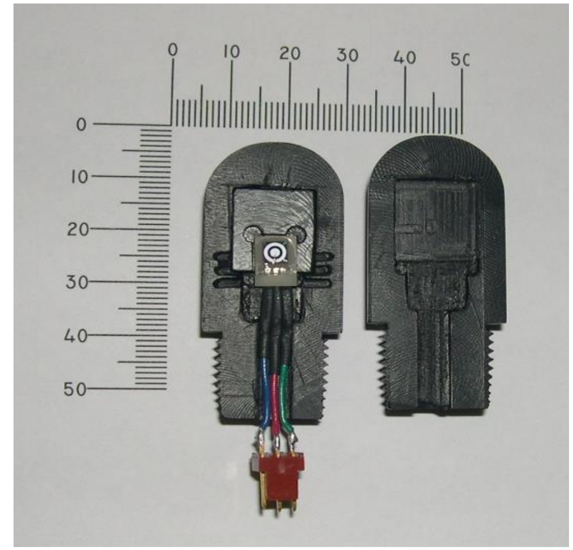

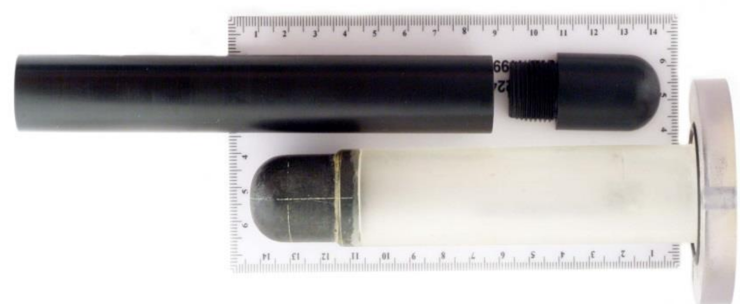

Measurements in Twin Detector Mode: single sensor for simultaneous g-n dosimetry

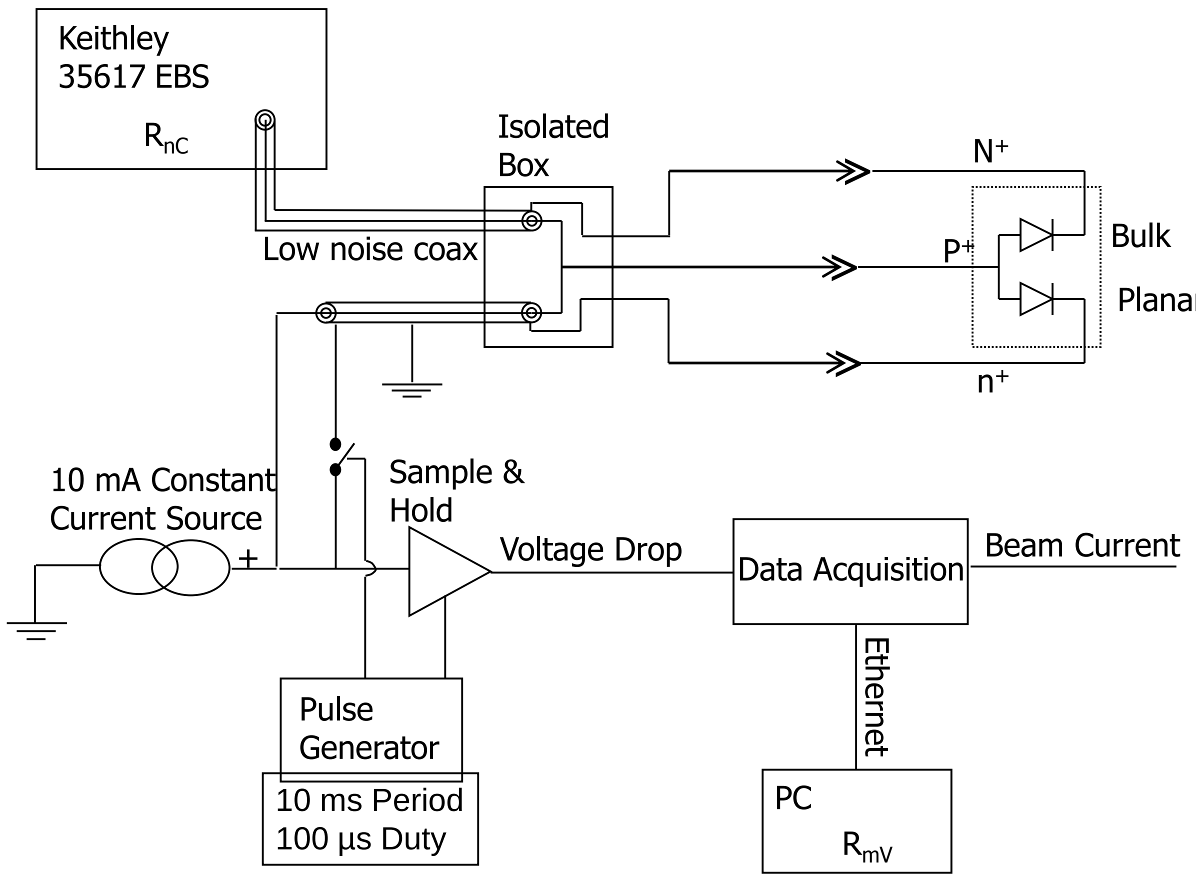

Neutron Sensitivity by Lead Attenuation Method

- The responses of the TE ionization chamber and the diode, R_{TE}, R_{mV} and R_Q, are measured in narrow beam geometry as a function of lead absorber thickness
- The responses are related to the lead thickness, t, and gamma ray attenuation coefficient, μ, as:

$$\overline{R} = \frac{R(t) - R(0)\cdot \exp(\mu \cdot t)}{1 - \exp(\mu \cdot t)}$$

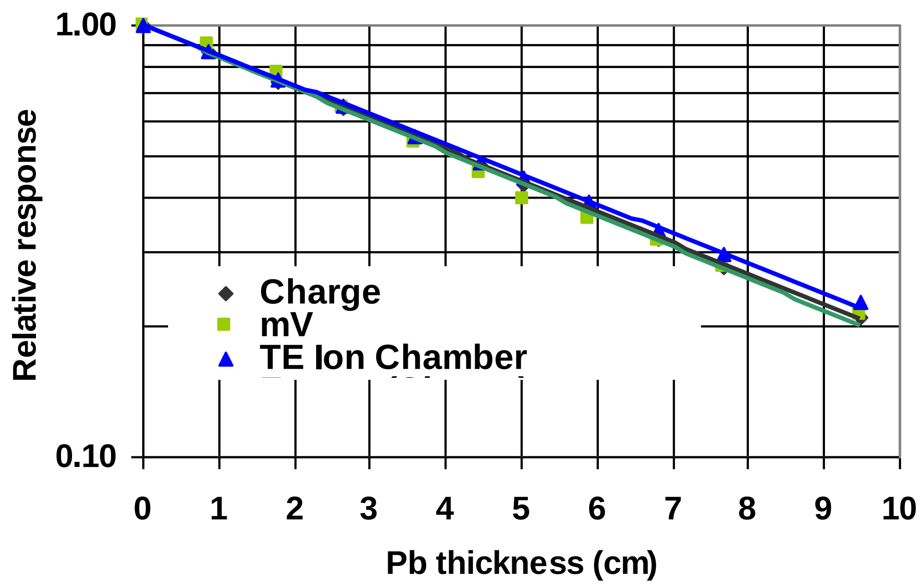

Neutron Sensitivity of the Diode Operated in the Voltage Drop Mode

- Linear relationship between the modified responses of TE ionization chamber and the diode:

$$\overline{R}_{TE} = \frac{k_T}{C_{n,mV}} \cdot \overline{R}_{mV} + D_{s,\gamma}$$

k_T is relative neutron sensitivity of TE ionization chamber

$k_T = 0.994$

$D_{s,\gamma}$ is the gamma dose due to the scatter arising from the shielding and surrounding

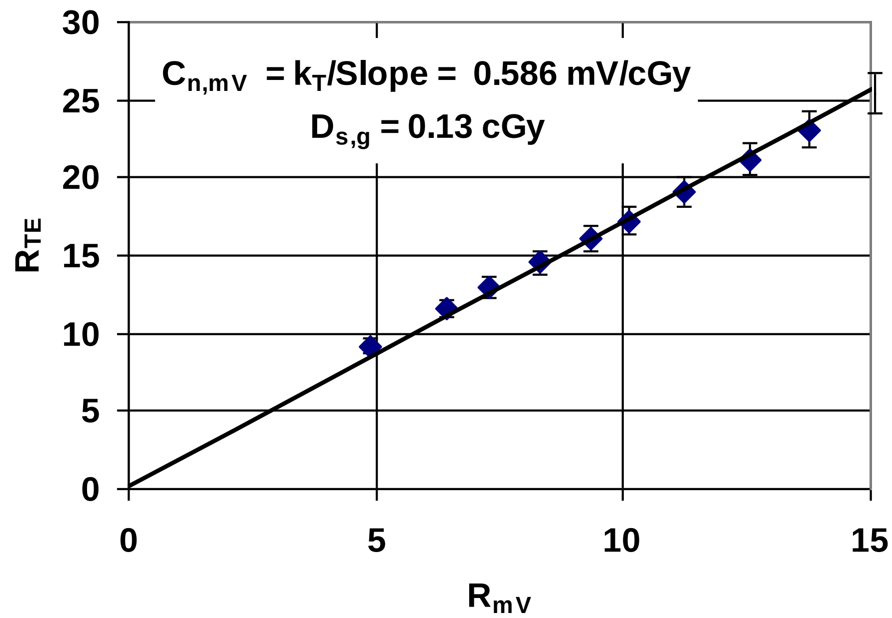

Neutron Sensitivity of the Diode Operated in the Charge Collection Mode

- Linear relationship between the modified responses of the diode and the TE ionization chamber is given by:

$$\overline{R}_Q = \frac{k_Q}{k_T}\left(\overline{R}_{TE} - D_{s,\gamma}\right) + D_{s,\gamma}$$

$$R_Q = \frac{R_{nC}}{C_\gamma} \quad \text{and} \quad k_Q = \frac{C_{n,nC}}{C_\gamma}$$

C_γ is obtained from the measurements in ^{60}Co beam

C_γ = 1.11 nC/cGy

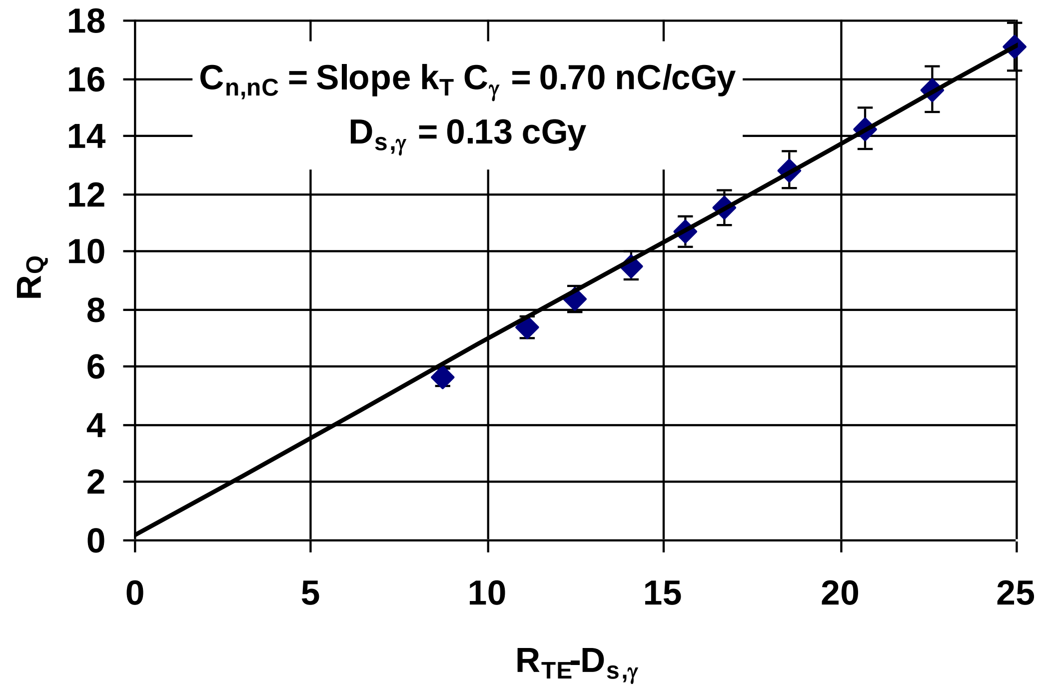

Lateral Neutron Dose Profile at 5 cm Depth in 10 × 10 cm^2 Field

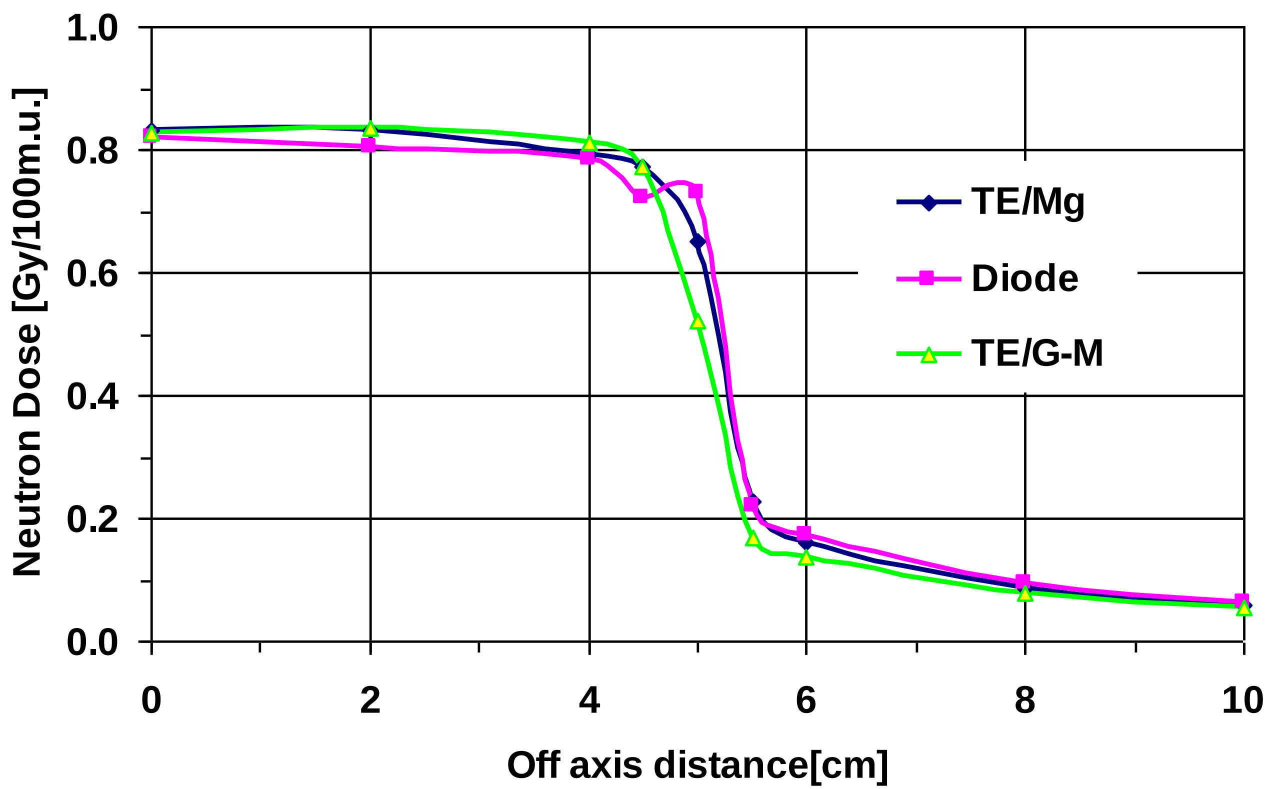

Lateral Profile of Total (Neutron + Gamma) Dose at 5 cm Depth in 10 × 10 cm^2 Field

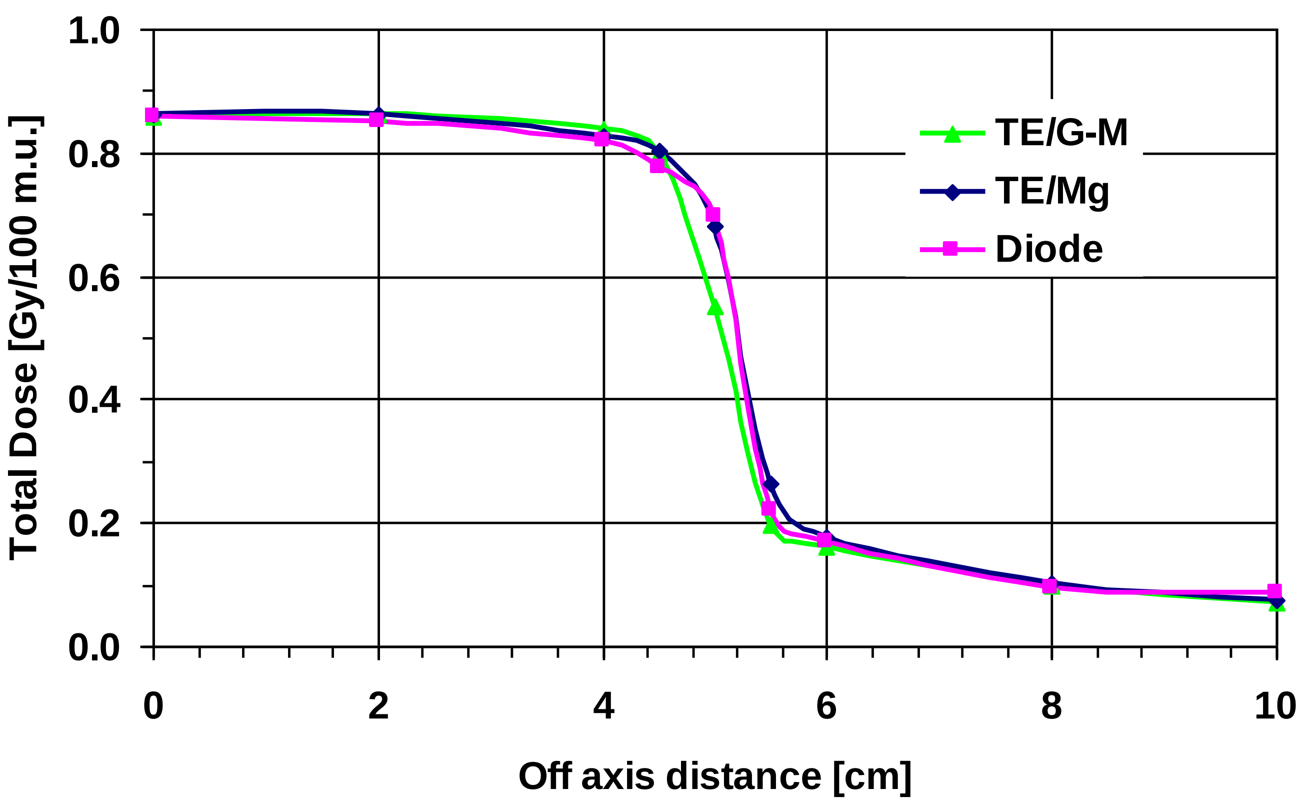

Neutron Depth Dose Along the Central Axis in 10 × 10 cm^2 Beam

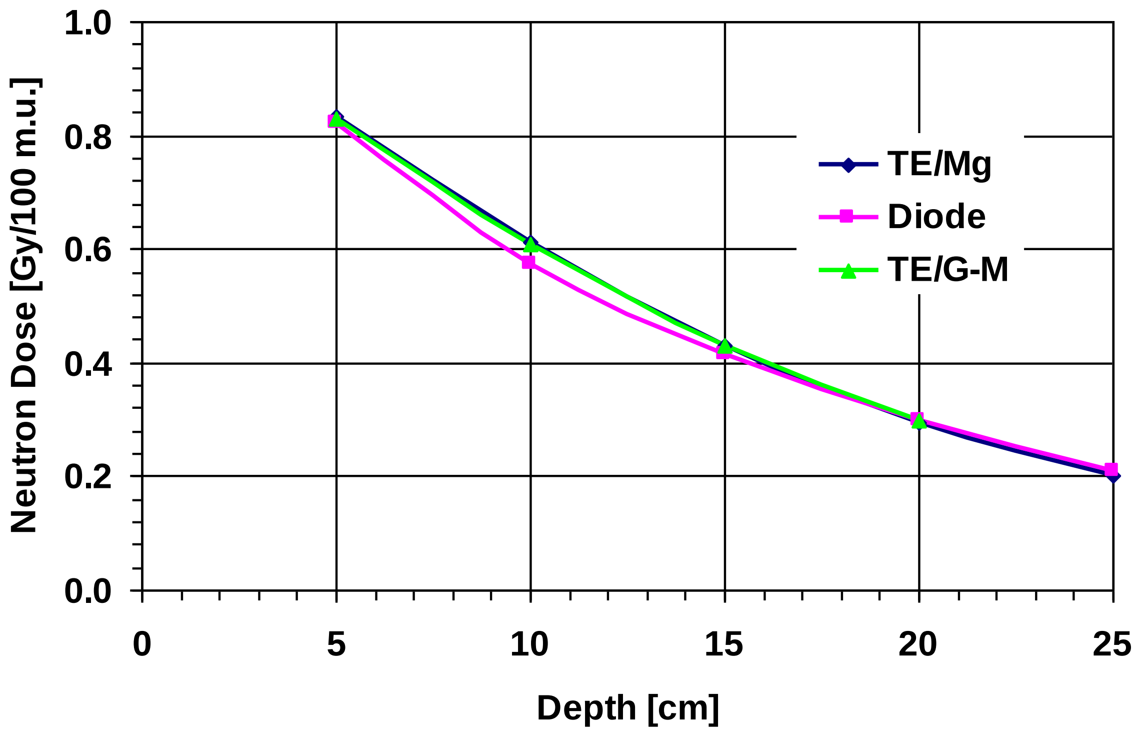

Total (Neutron + Gamma) Depth Dose Along the Central Axis in 10 × 10 cm² Beam

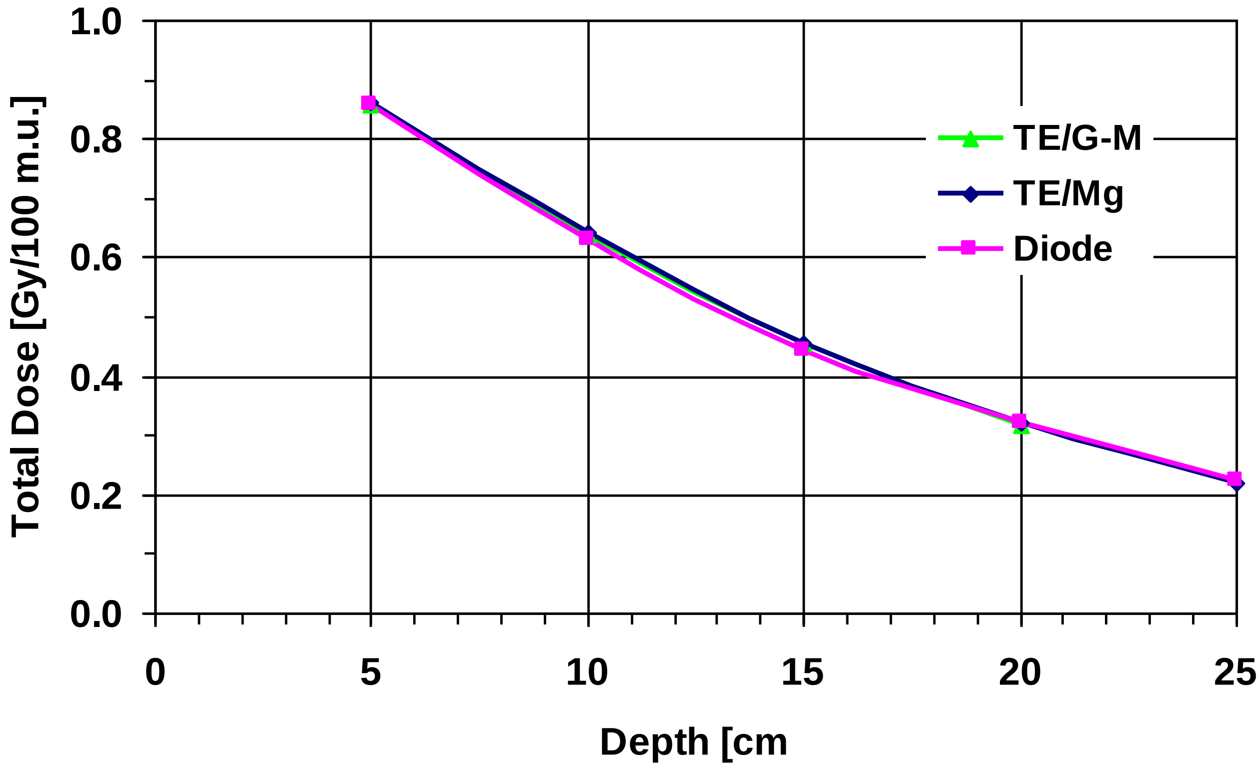

TE/G-M Diode Comparison in 15 × 15 cm² Field

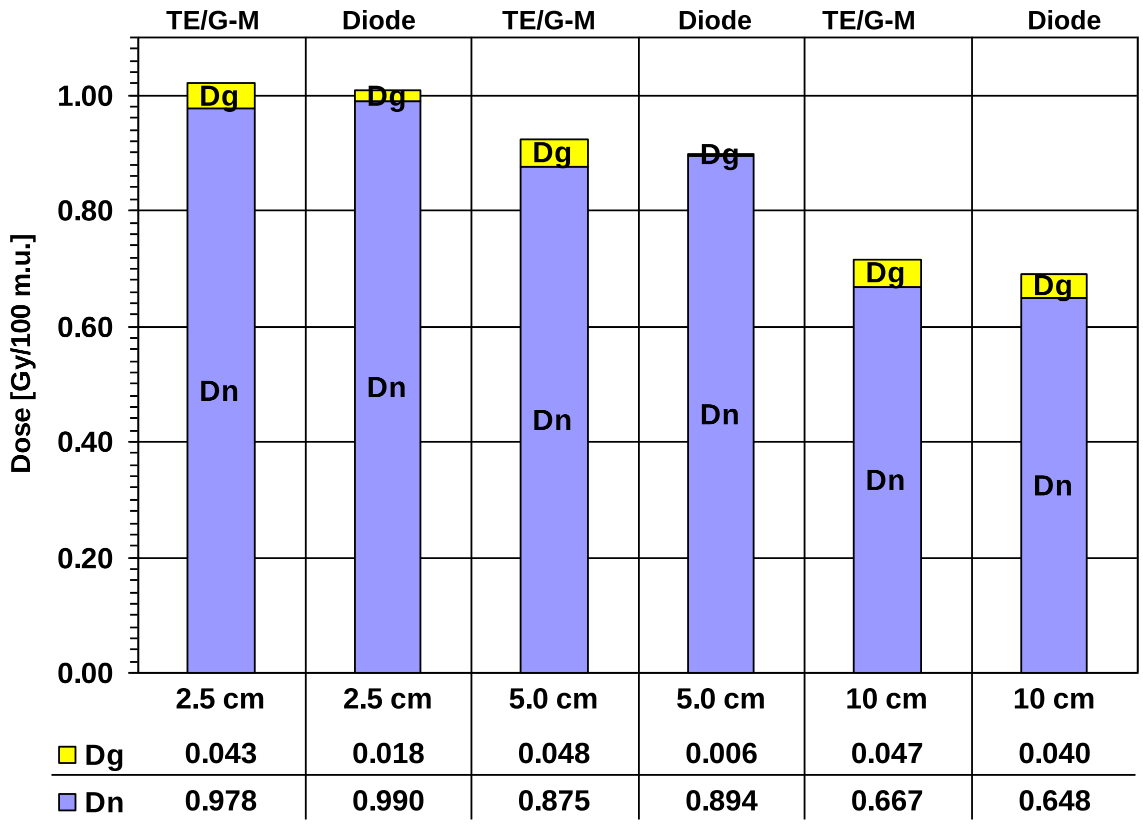

TE/G-M Diode Comparison in Blocked Beam

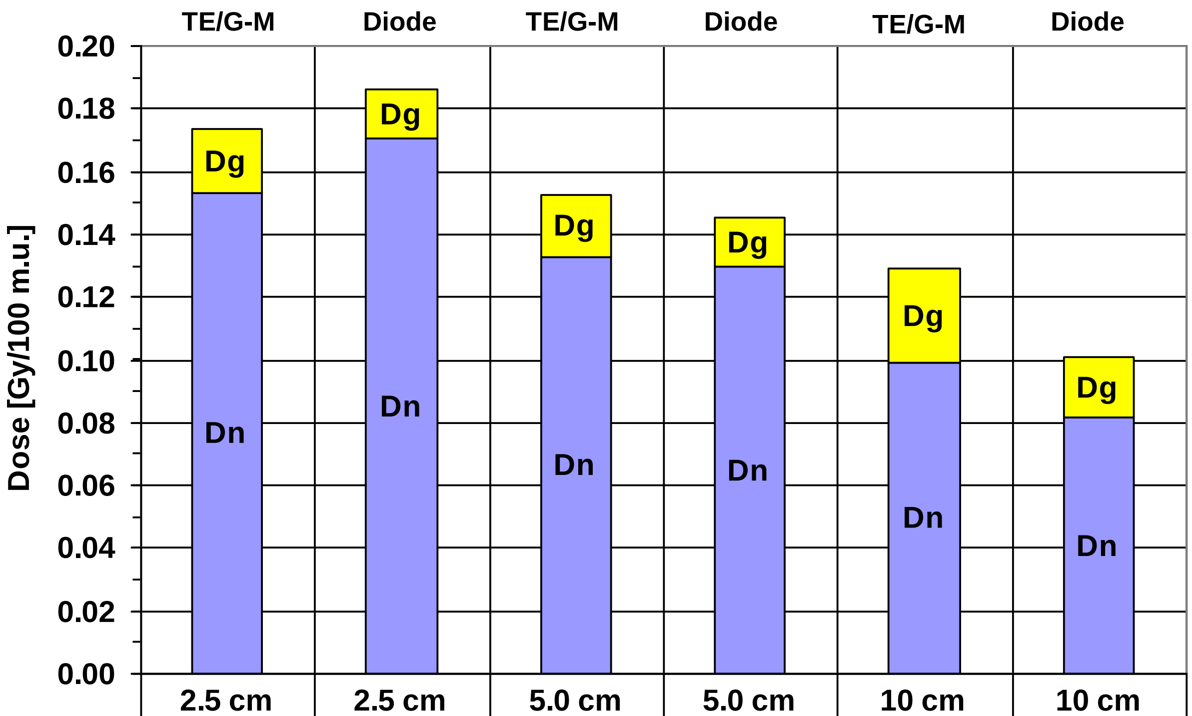

	2.5 cm	2.5 cm	5.0 cm	5.0 cm	10 cm	10 cm
Dg	0.020	0.016	0.020	0.016	0.030	0.019
Dn	0.153	0.171	0.133	0.130	0.099	0.082

Conclusion

- Application of ion implanted *p-I-n* diodes of novel design was investigated in fast neutron beam
- Operation of the device in “voltage drop” and “charge collection” modes makes it suitable as a twin detector for dosimetry of mixed neutron/gamma beams
- The sensitivity to neutrons and gamma for both “voltage drop” and “charge collection” modes was defined by the lead attenuation method
- Total dose together with separate neutron and gamma components were measured at different beam locations as well as under partially blocked collimator
- The results compare favorable with those obtained with paired TE ionization chamber and G-M counter
- Further investigation is underway for application of the method in clinical practice

MOSFET detector Mini- Micro-Dosimetry: generation 1

Simultaneous measurements of stochastic (microdosimetry) and deterministic (absorbed dose) effects at the same location: History of Si Microdosimetry , 1995

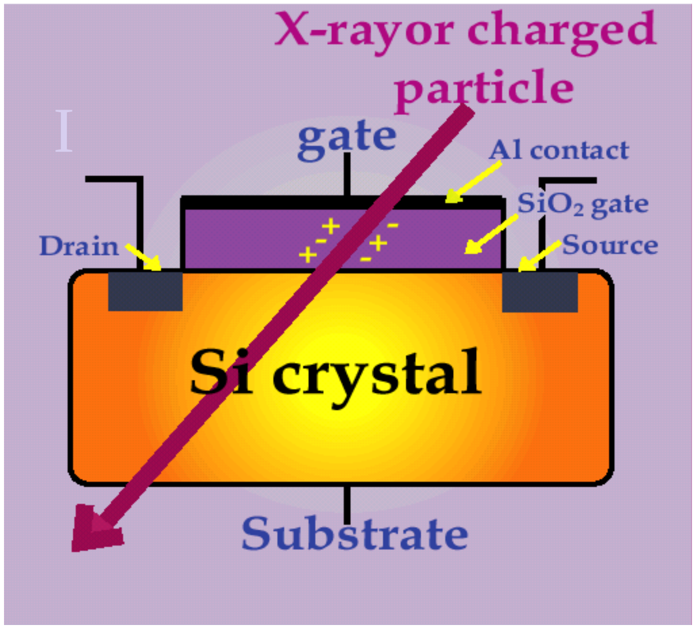

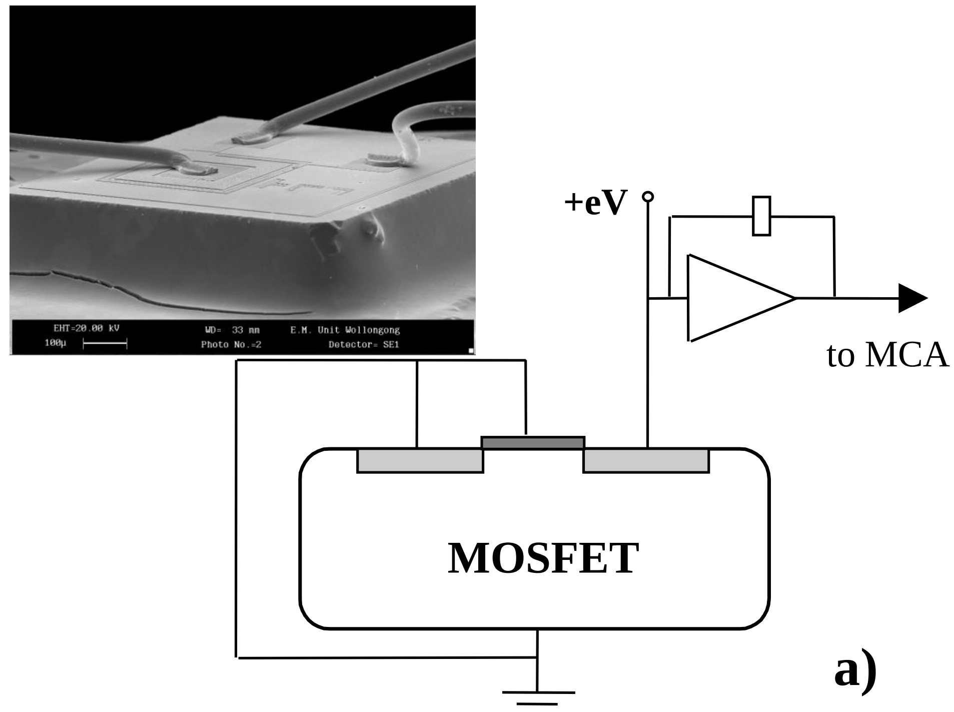

$$\Delta V_{th} = -\frac{eg}{\varepsilon_{ox}\varepsilon_0} x_c \cdot d_{ox} \cdot f \cdot P \cdot D$$

$$\Delta V_{th} \propto D$$

A.Rosenfeld et al. “Simultaneous Macro and Micro Dosimetry with MOSFET” , IEEE TNS **43**, 2693, 1996

CENTRE FOR MEDICAL RADIATION PHYSICS | UNIVERSITY OF WOLLONGONG

MOSFET detector Mini- Micro-Dosimetry: generation 1

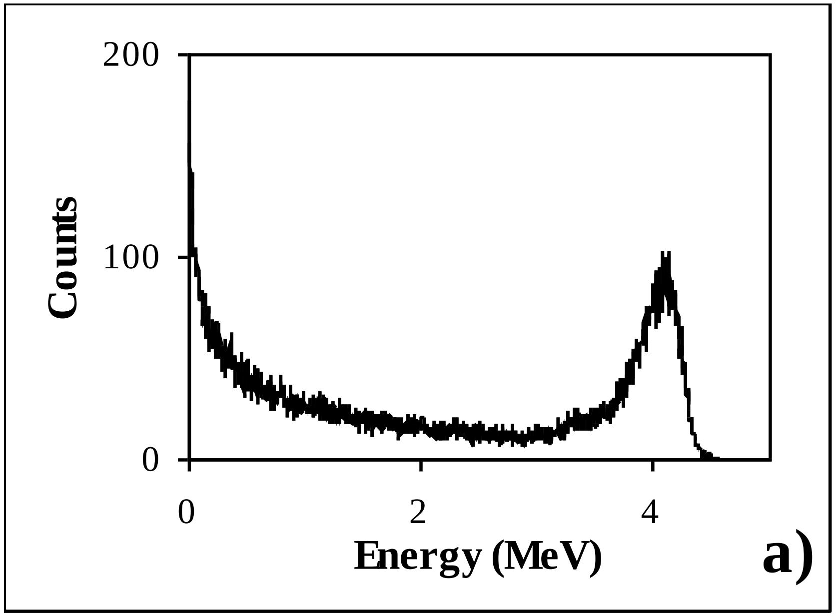

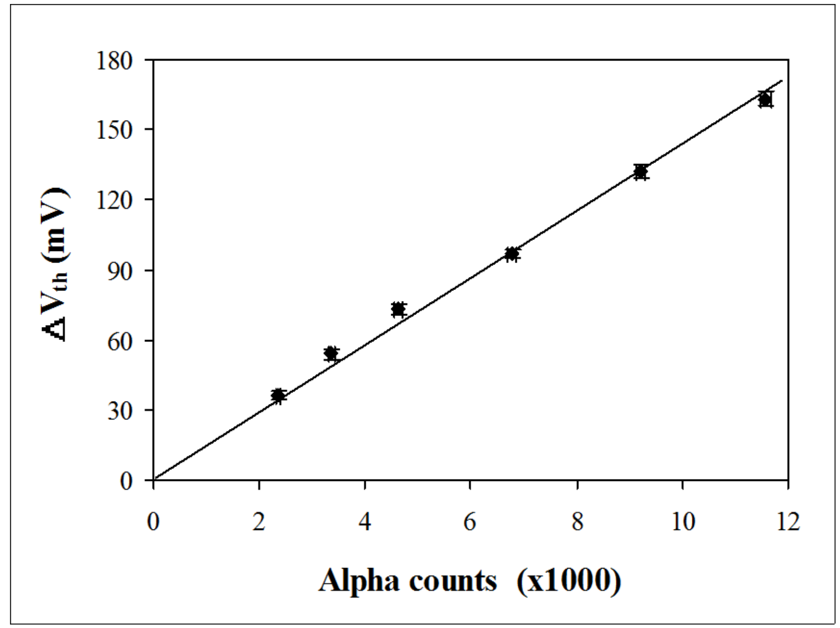

Pulse height spectrum of ^{241}Am alpha particles deposited at drain p-n junction

MOSFET threshold voltage change versus number of alpha particles registered in count mode by the same MOSFET

MOSFET detector Mini- Micro-Dosimetry

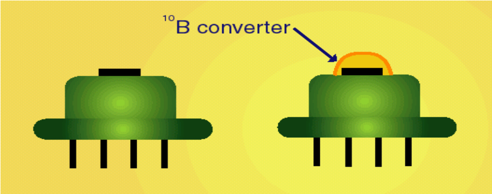

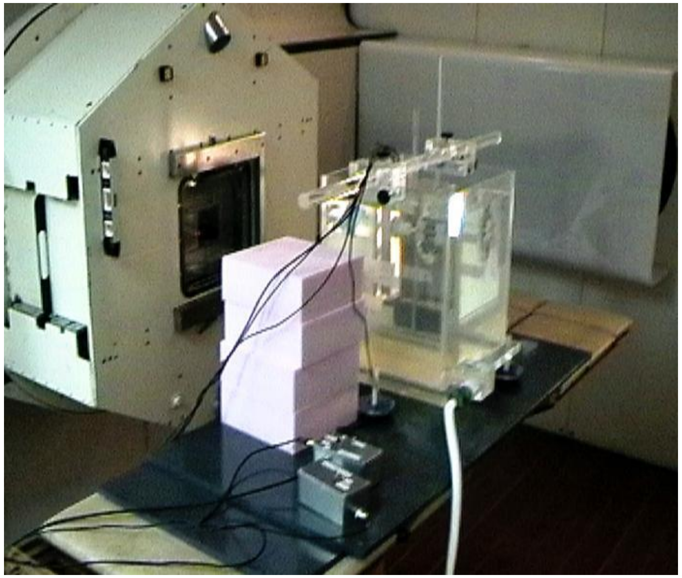

FNT facility with MOSFET probe in a water phantom, radiation field 10x10 cm2

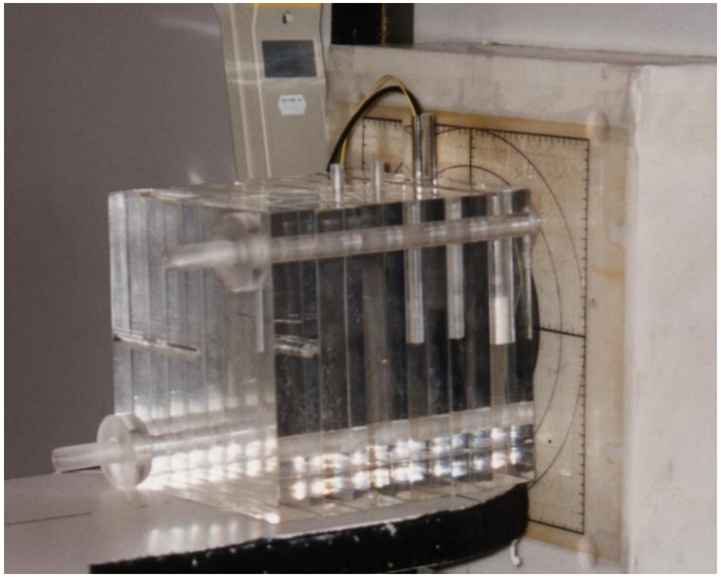

PMMA slab phantom placed next to the collimator of the epithermal neutron irradiation facility of the BMRR

MOSFET detector Mini- Micro-Dosimetry: FNT

- Experiments in a water phantom at FNT facility , USA
- Average neutron energy 20.4MeV, 10x10 cm^2 field
- MOSFET probe: simultaneous readout of single event spectra N(E) from the drain p-n junction and relative absorbed dose (Vth)at different depth

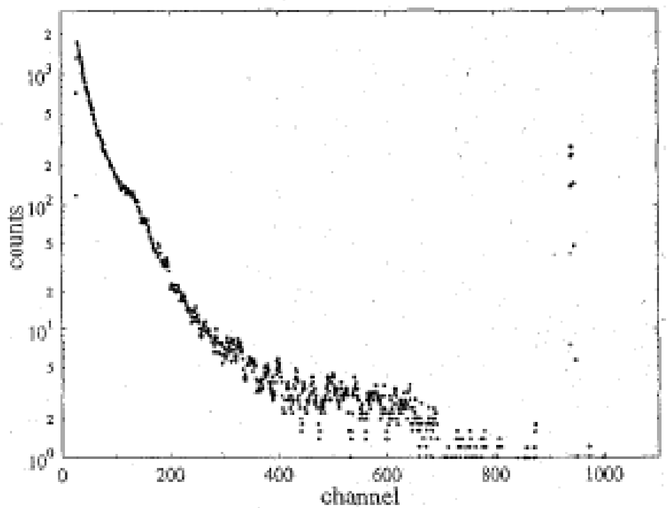

Fig 6. Pulse height spectrum obtained at a depth of 15 cm in the water phantom exposed in FNT neutron beam.

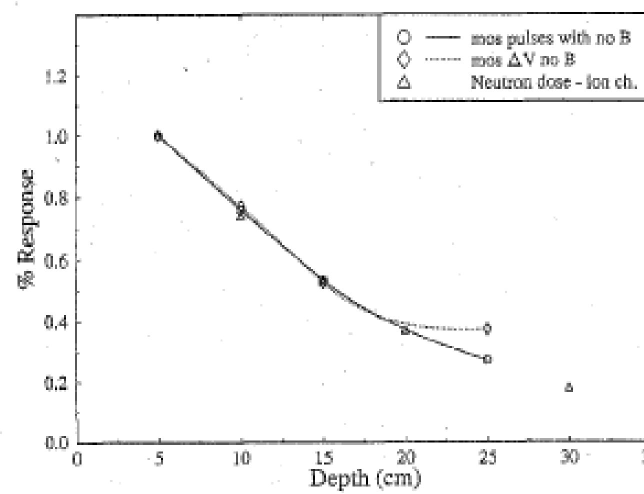

Fig 9 Threshold voltage change of the MOSFET at different depths in the water phantom when exposed in the FNT neutron beam.

Microdosimetry with a single micro SV

- RPP SV 100x100x20 μm3 including diffusion
- Funneling effect-uncertainties in SV
- Single only SV, efficiency is low
- Impossible represent cells array

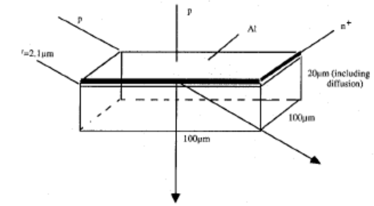

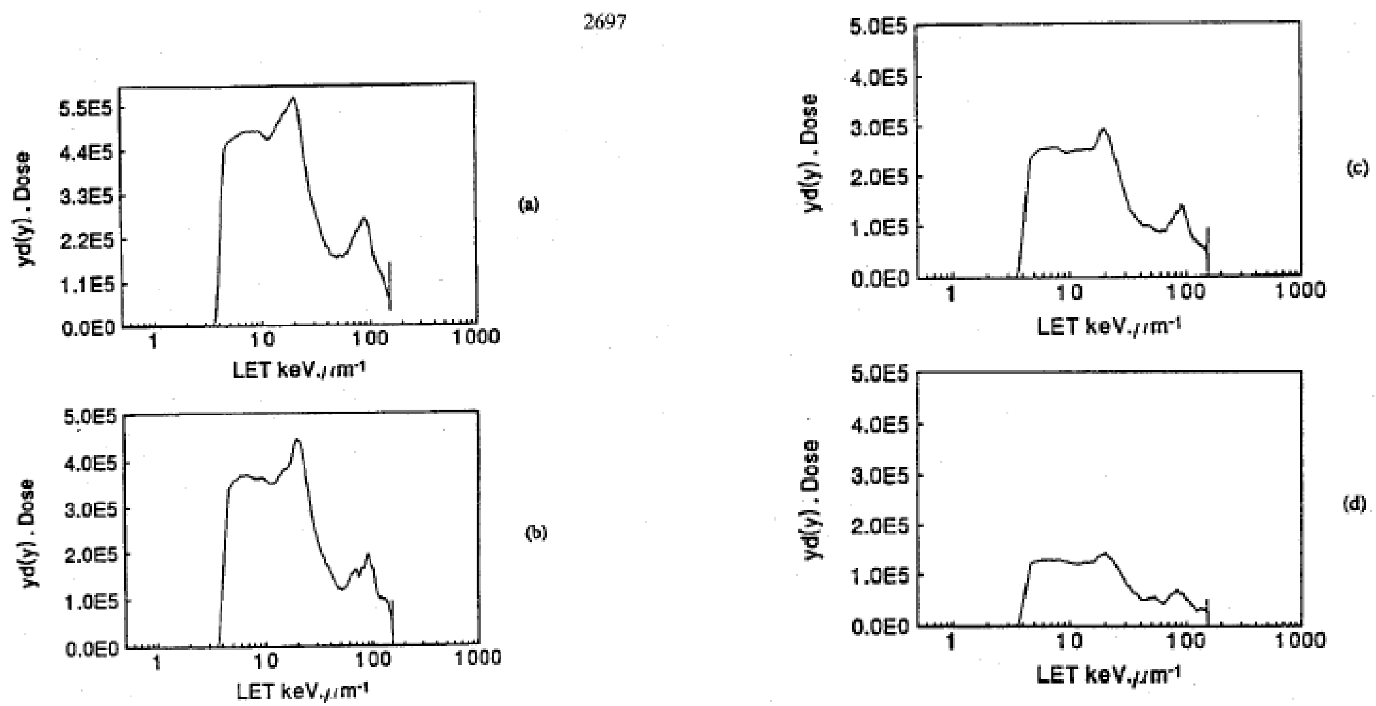

Microdosimetric spectra at FNT : depths 5, 10, 15, 20 cm in water

Future of Accelerator Based BNCT NIS using Liquid Lithium Target

$$^{10}\mathrm{B} + n \overset{94\%}{\rightarrow} \alpha\ (1.47\,\mathrm{MeV}) + {}^{7}\mathrm{Li}\ (0.84\,\mathrm{MeV}) + \gamma\ (0.48\,\mathrm{MeV})$$

$$\overset{6\%}{\rightarrow} \alpha\ (1.78\,\mathrm{MeV}) + {}^{7}\mathrm{Li}\ (1.01\,\mathrm{MeV})$$

1988 - 1996: Updating neutron irradiation system for BNCT using KUR

T.Kobayashi, Y.Sakurai, K.Kanda, Y.Fujita and K.Ono, "The Remodeling and Basic Characteristics of the Heavy Water Neutron Irradiation Facility of the Kyoto University Reactor Mainly for Neutron Capture Therapy", *Nuclear Technology,* 131 (2000) 354-378.

1988-89 The repair of HWTNF for the leakage of heavy water from the storage tank.

1990-94 A design study for thermal and epi-thermal neutron irradiation system for BNCT. A Reactor BNCT neutron irradiation system was established.

1995-96 Updating; The convenience of the irradiation technique was improved.

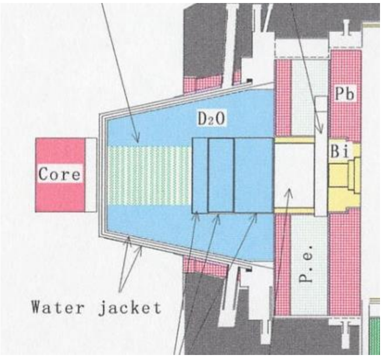

BSA of HWNIF (new)

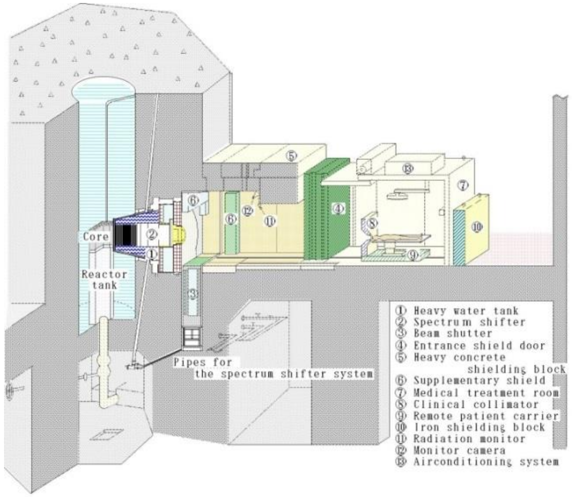

An isometric view of the HWNIF

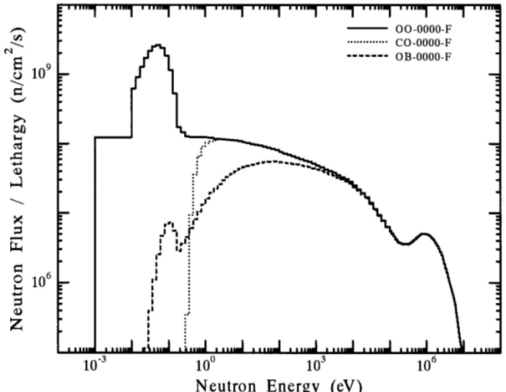

Neutron energy spectrum

Courtesy of Prof T. Kobayashi

CENTRE FOR MEDICAL RADIATION PHYSICS | UNIVERSITY OF WOLLONGONG

Cyclotron Based Epi-thermal Neutron Source(C-BENS)

Pb : used as a breeder and a reflector for high energy neutrons
Fe : used as a moderator
Al and CaF_2 : used as a shaper for epi-thermal region
Polyethylene : used as a shielding for high energy neutrons

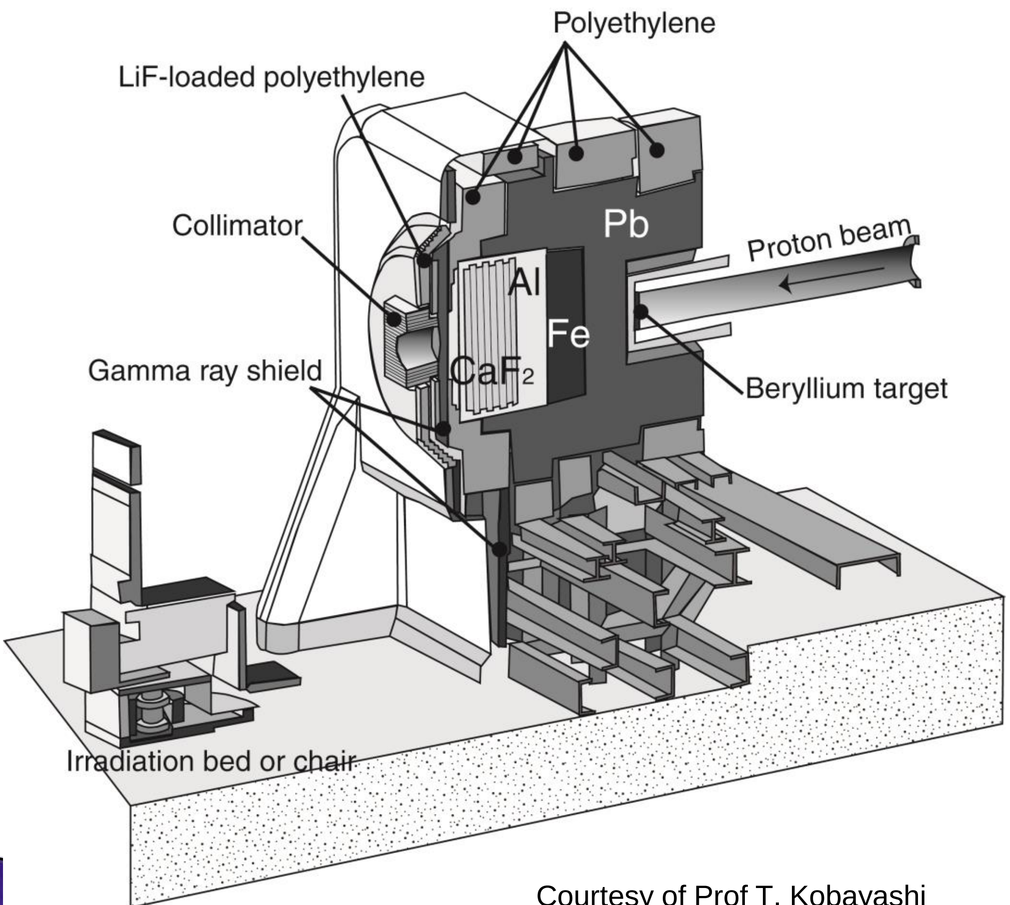

Courtesy of Prof T. Kobayashi

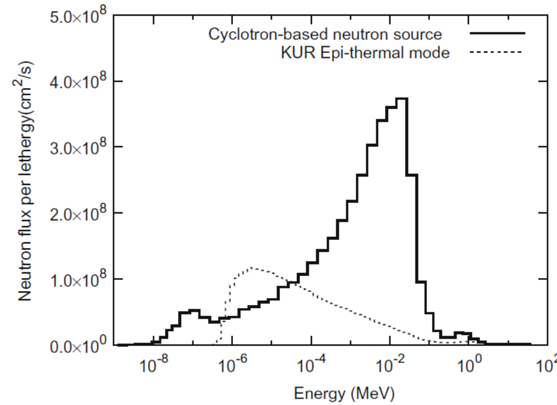

Fig. 6. Comparison with neutron spectrum at a gamma shield for KUR and CBNS.

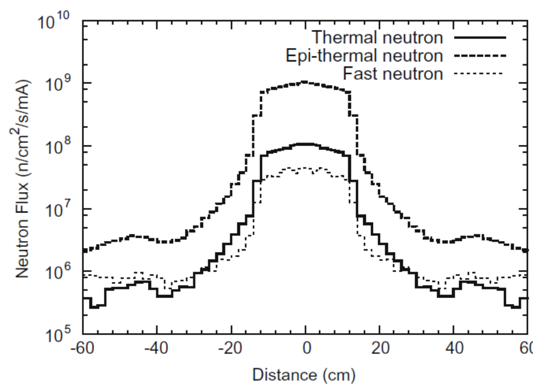

Fig. 7. Flux distribution of thermal, epithermal and fast neutrons as a function of distance from beam axis.

MOSFET Neutron Dosimetry in BNCT

- Measurement of thermal neutron flux distribution in a phantom is important for the verification of the dose planning system
- Measurements of real “Boron-10” response is an advantage as the cross section of Boron-10 is proportional to 1/V
- Online dosimetry using paired MOSFET detectors, both identical detectors produced on the same chip, with one of them covered with the Boron-10 converter

Paired MOSFET detectors without and with ^{10}B Perspex converter

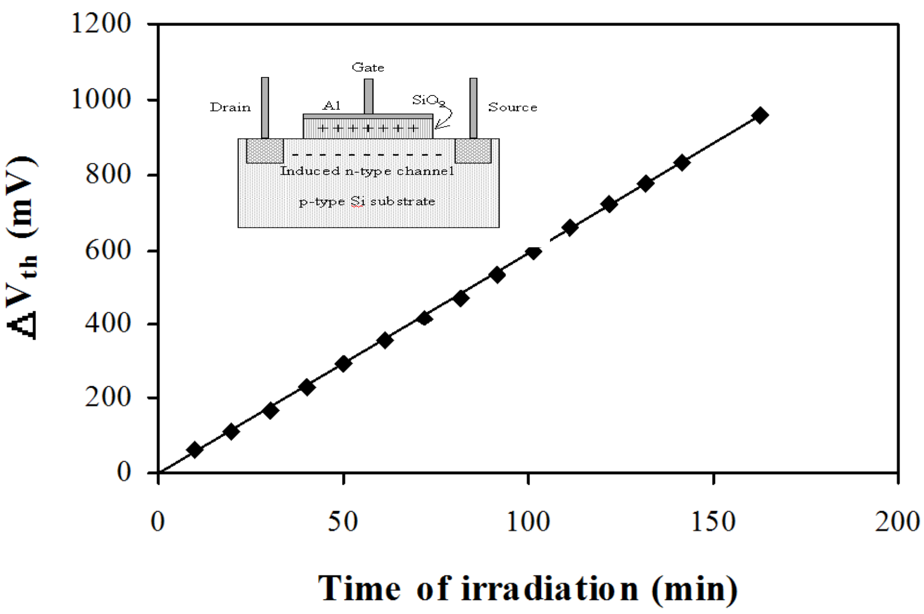

The integral response of an n-MOSFET with a thick oxide layer about 1 micron to 5.48 MeV alpha particles from ^{241}Am with a fluence of about 4×10^{3} $cm^{-2}s^{-1}$

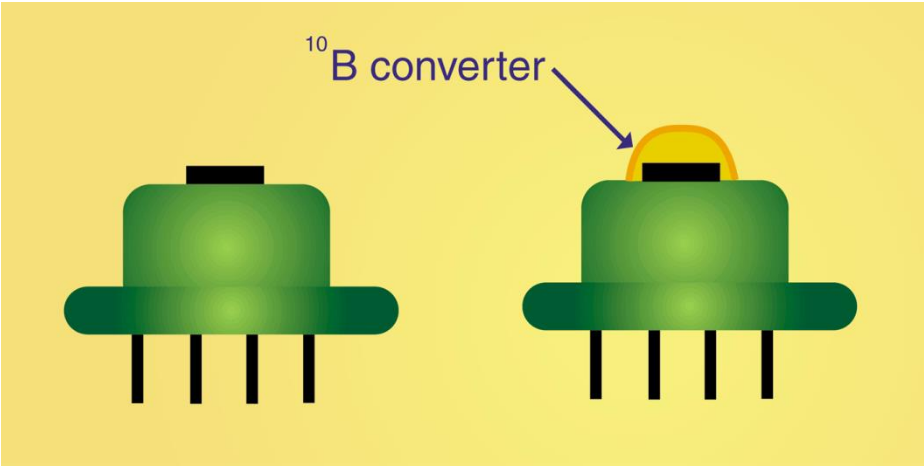

Thermal Neutron Fluence
$F = A(\Delta V_{B-10} - \Delta V)$

CENTRE FOR MEDICAL RADIATION PHYSICS
UNIVERSITY OF WOLLONGONG

BNL Epithermal BNCT Facility, Head Phantom

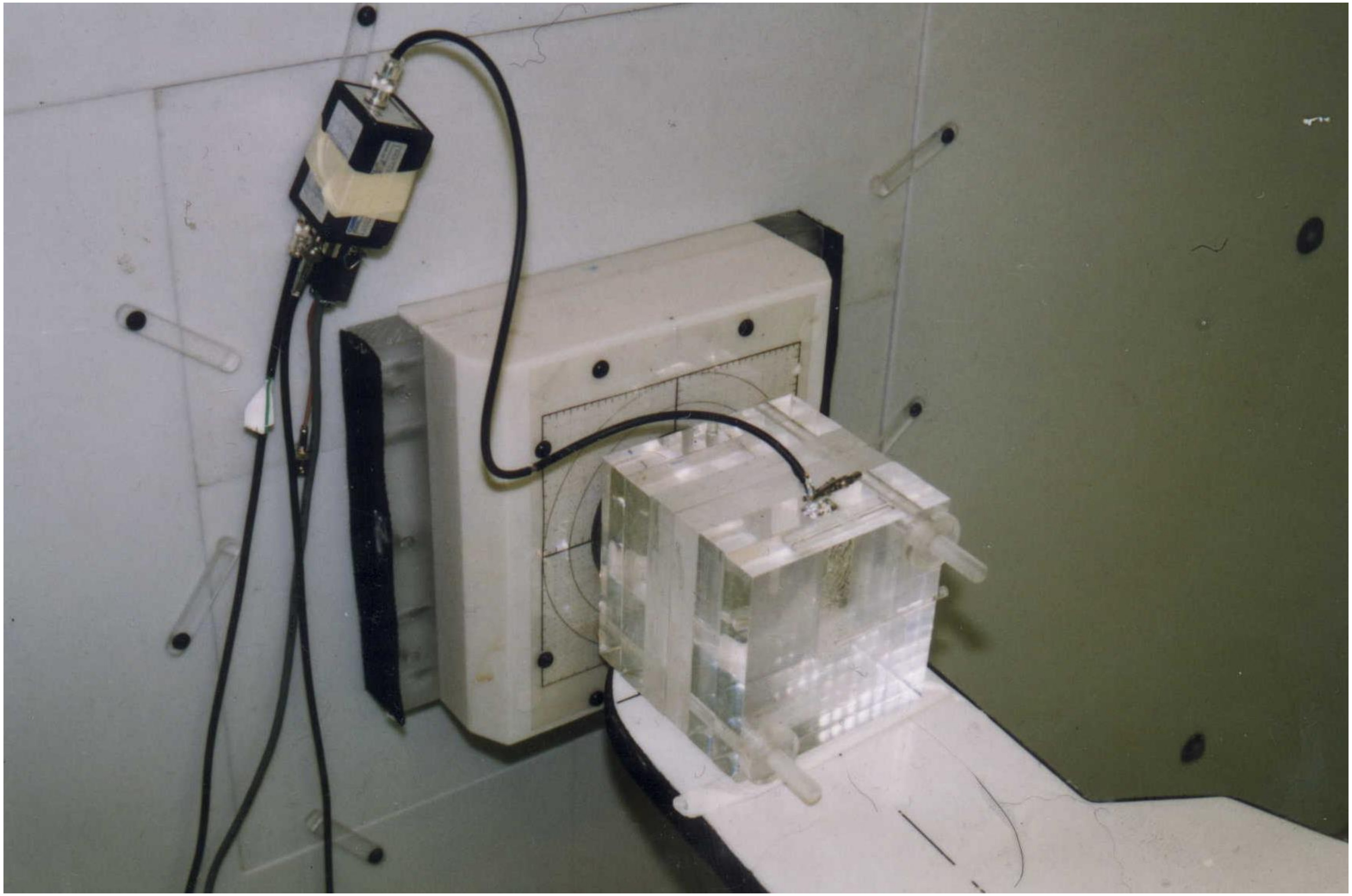

BNCT at BNL medical research reactor

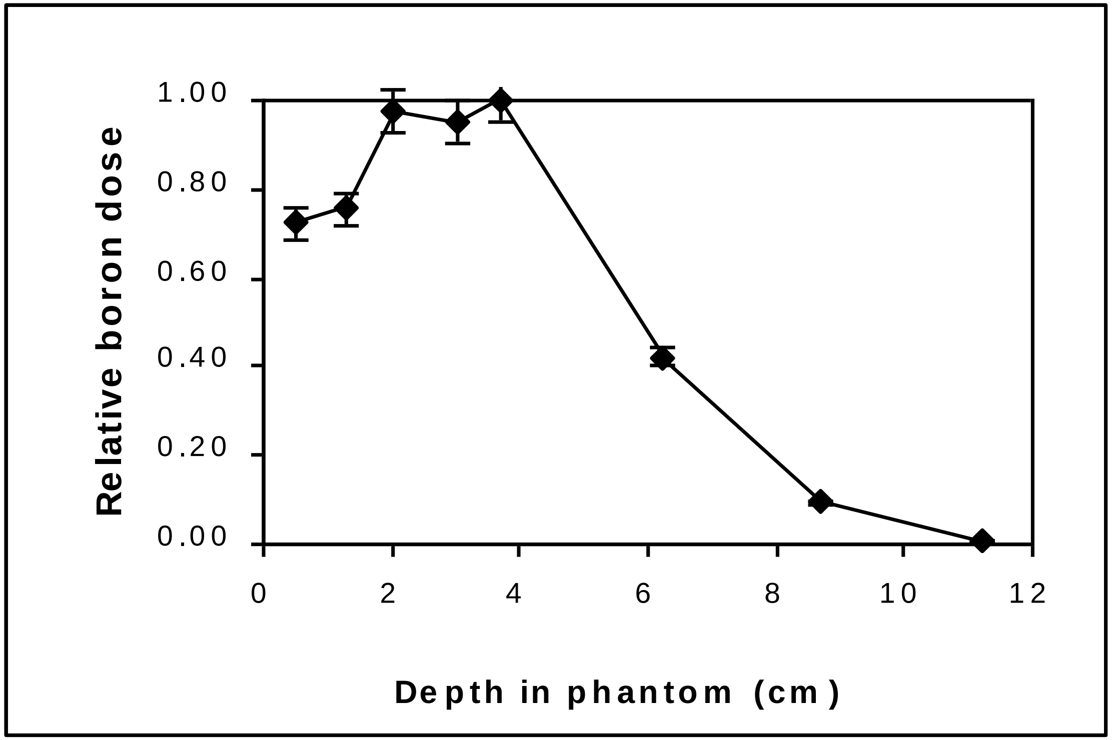

- Boron depth dose distribution in a Perspex phantom in a BNCT epithermal neutron beam facility at BNL obtained paired MOSFET detectors with ^{10}B converter

p-i-n Detector with U-235 Converter

Fission Detector

^{235}U captures a thermal neutron and fissions with a probability of 85%. The ^{235}U nucleus splits in about 40 modes. A typical nuclear reaction is

$$ {}_{0}^{1}n + {}_{92}^{235}U \rightarrow {}_{57}^{147}La + {}_{35}^{87}Br + 2\,{}_{0}^{1}n $$

Two fragments carry total kinetic energy of 162 MeV

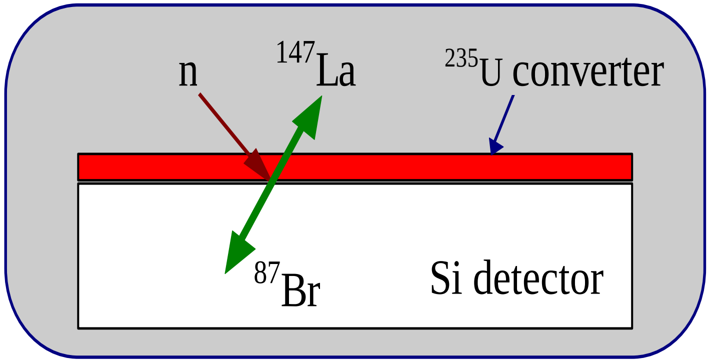

^{235}U Converter on Silicon Detector

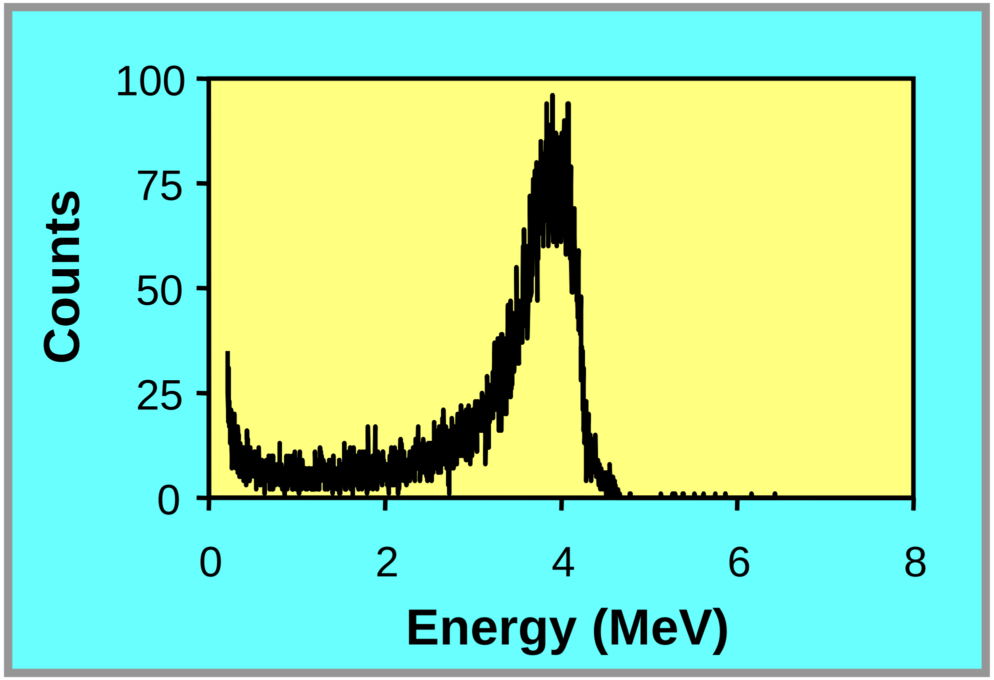

Spectrum of spontaneous alpha decay of ^{235}U of the fission coverter

Alpha peak was used for on-line energy calibration and measuring activity of the converter

Epithermal BNCT at BMRR.

Pulse height spectra in 15x15x15 cm Perspex phantom

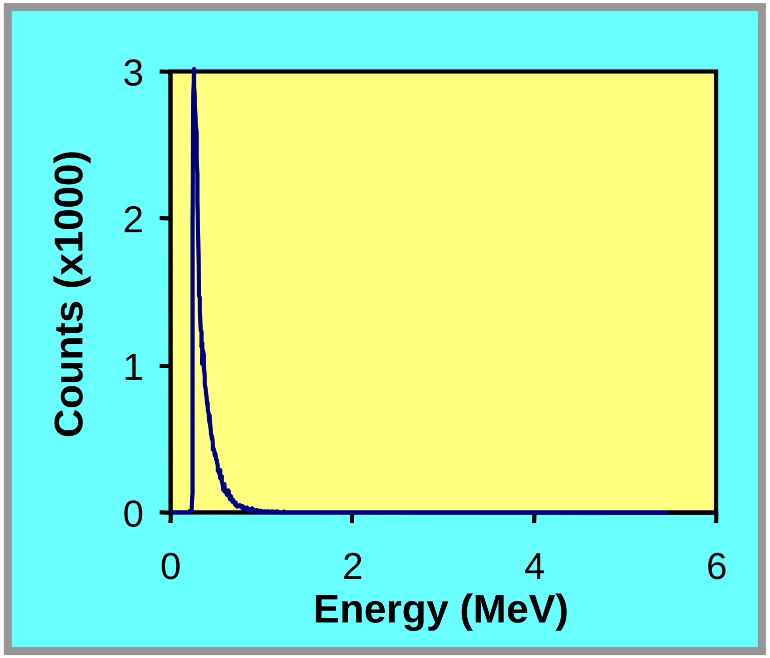

Silicon detector spectrum, without the fission converter, at 3.7 cm depth in the phantom

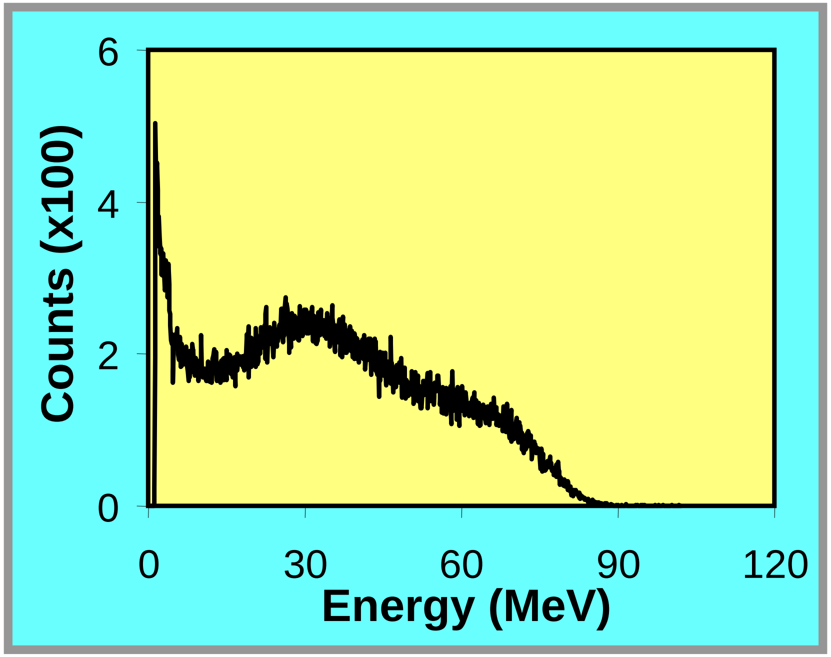

Fission detector spectrum at 3.7 cm depth in the phantom

Epithermal BNCT at BMRR.

Pulse height spectrum in 15x15x15 cm Perspex phantom

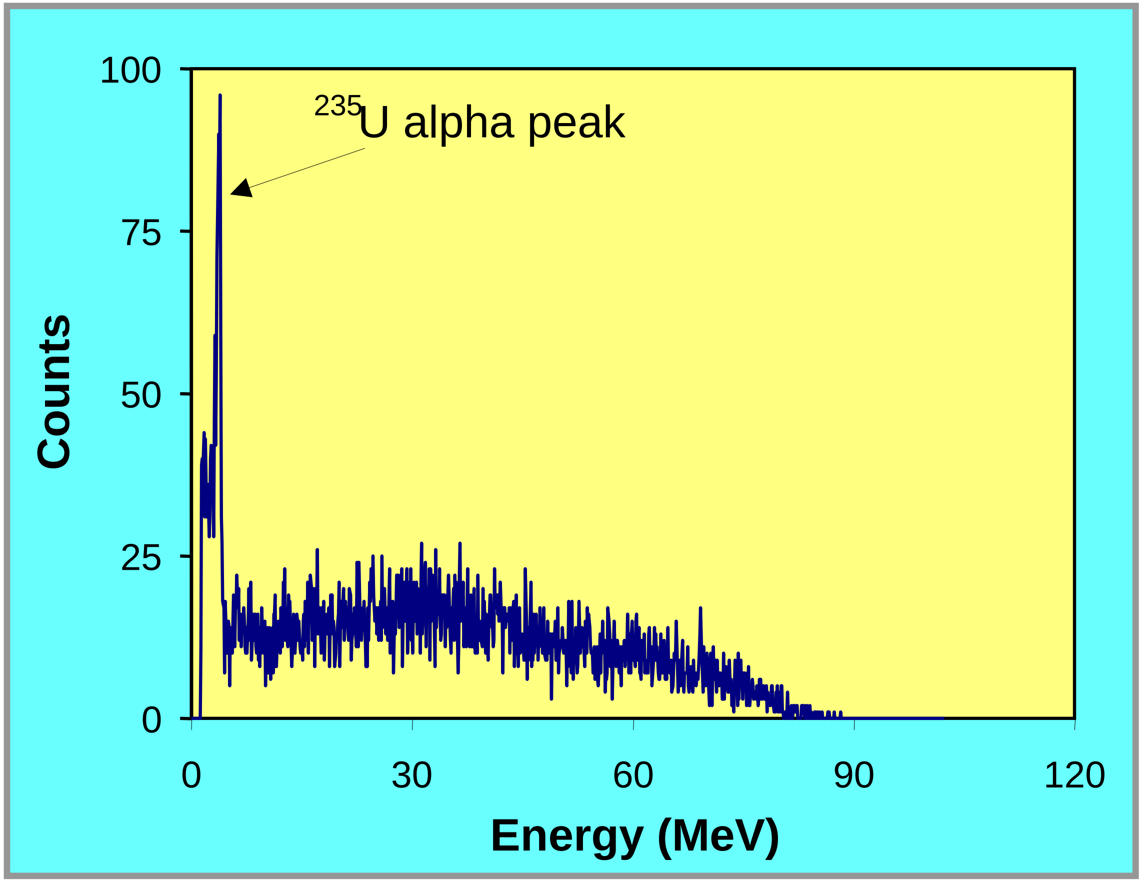

Thermal neutron fluence is given by

$\phi = N_f / (\sigma . N_u . p)$

p=0.85 is the fission probability

N_u is the number of U-235 converter

N_f is the number of fragments – area under the spectrum

σ is the cross section

Fission detector spectrum at 11 cm depth in the phantom

Thermal Neutron Flux in Perspex Phantom

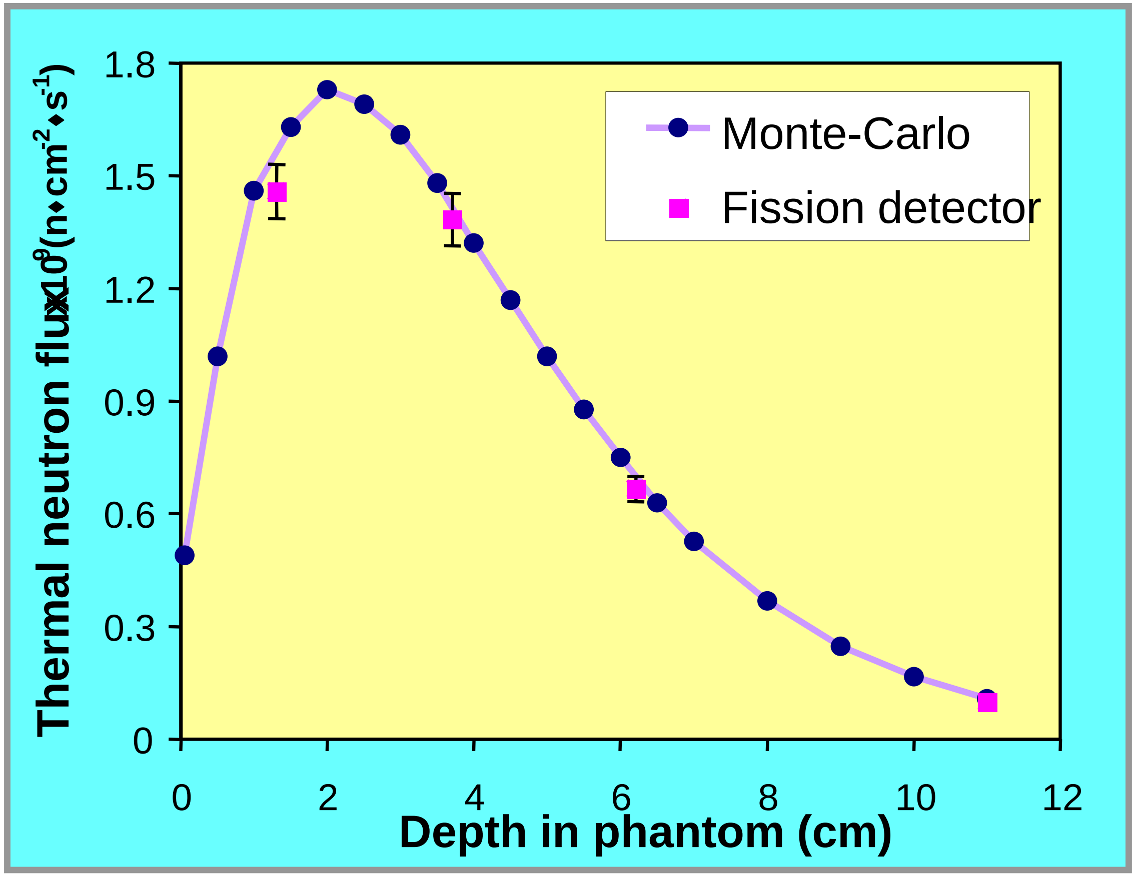

Monte Carlo calculated and fission detector measured thermal neutron flux along the Perspex phantom central axis. BMRR, BNCT facility, 3 MW.

On Line Boron Dose Dosimetry in BNCT

BNCT System

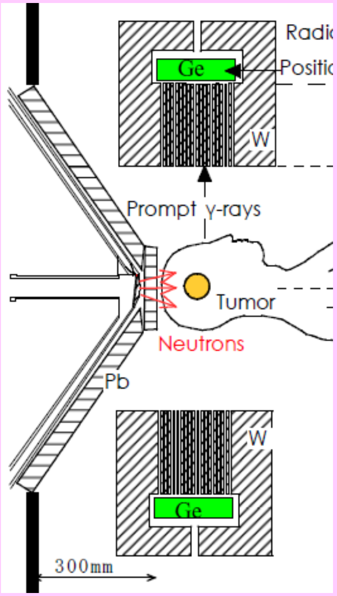

- **Pb shielding: 3cm**
- **PG-SPECT: On-line dose monitoring system**

Courtesy of Prof T. Kobayashi

$$^{10}\mathrm{B} + n \xrightarrow{94\%} \alpha\,(1.47\,\mathrm{MeV}) + {}^{7}\mathrm{Li}\,(0.84\,\mathrm{MeV}) + \gamma\,(0.48\,\mathrm{MeV})$$

$$\xrightarrow{6\%} \alpha\,(1.78\,\mathrm{MeV}) + {}^{7}\mathrm{Li}\,(1.01\,\mathrm{MeV})$$

Non-Tissue Equivalent Detectors for Monte Carlo Verification

- *p-i-n* diodes have been found to be useful for the verification of Monte Carlo simulation of phantom neutron spectra in epithermal BNCT
- Approach-
  - Running MCNP to simulate the neutron spectra at any depth in the phantom
  - Simulate damage kerma at any point in the phantom using simulated spectrum
  - Verify damage kerma experimentally through the placement of diodes in the phantom which are calibrated in terms of damage kerma

$$\Delta V=\alpha \int_0^E K(E_n)\, \Phi(E_n)\, dE_n$$

$K(E_n)$ is based on ASTM data
$F(E_n)$ the neutron spectra of HB 11 beam at the point of irradiation in free air geometry
a is a calibration coefficient
DV is a forward voltage shift of Si diode under investigation

Experiment at HB11 Epithermal Beam, Patten

- The simulated dose rate at the point of calibration was 0.576 cGy(Si) h^{-1} and determined the average calibration factor as being 214.9 mV cGy^{-1}(Si) with a 5% spread across 14 diodes

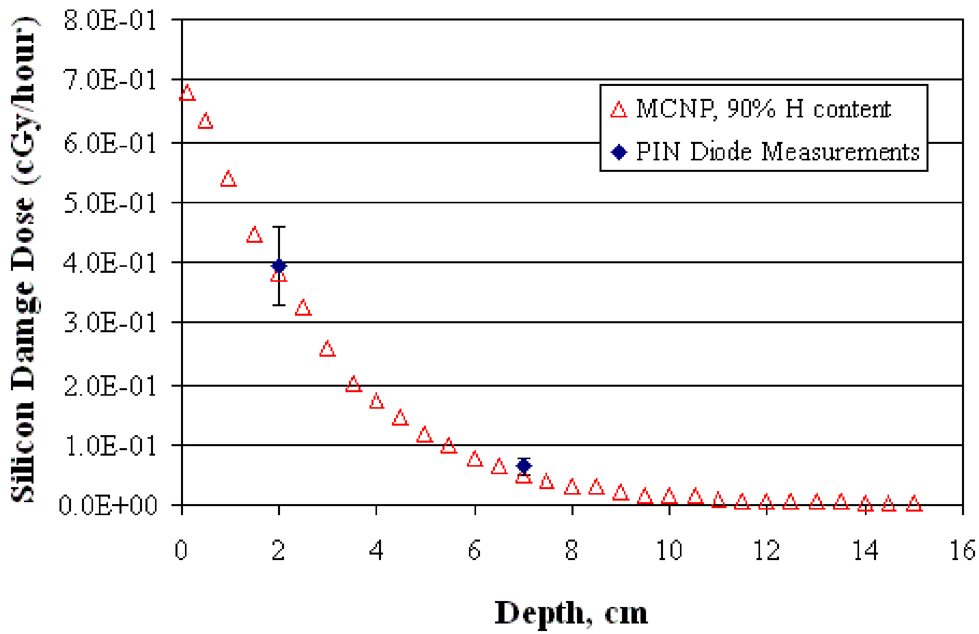

3D SOI silicon microdosimetry

- 3D silicon cell array for modeling of energy deposited in biological cells event by event by secondaries
- Each Si cell is 6x10 microns

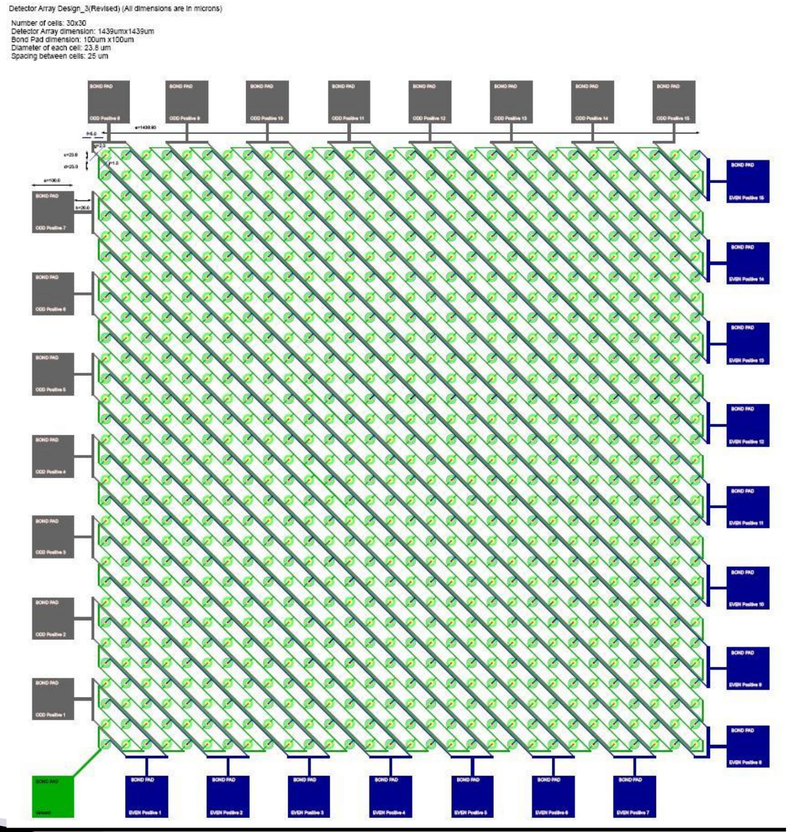

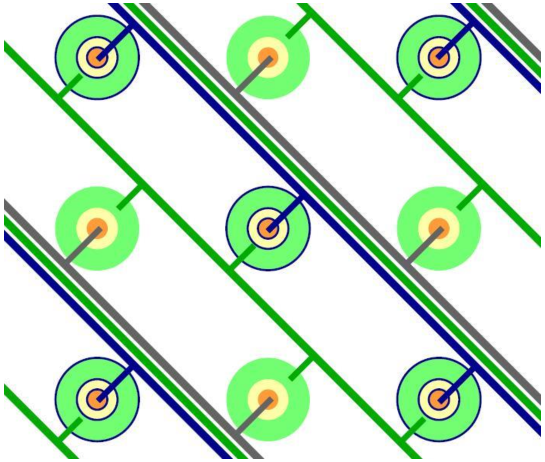

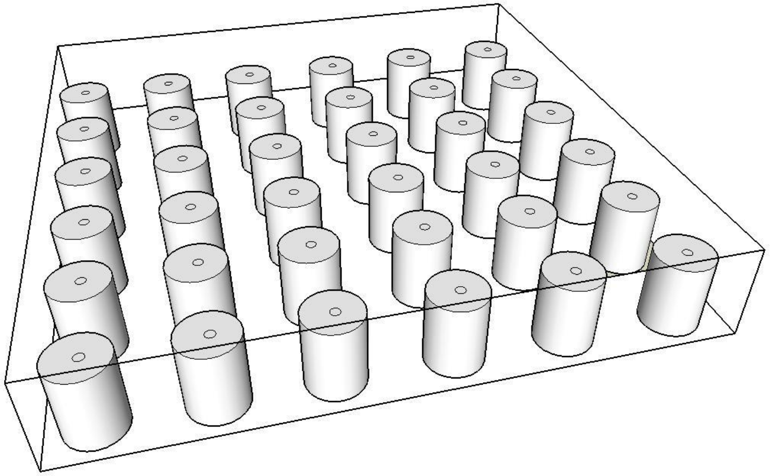

SOI Microdosimertry on 100 MeV Proton Therapy

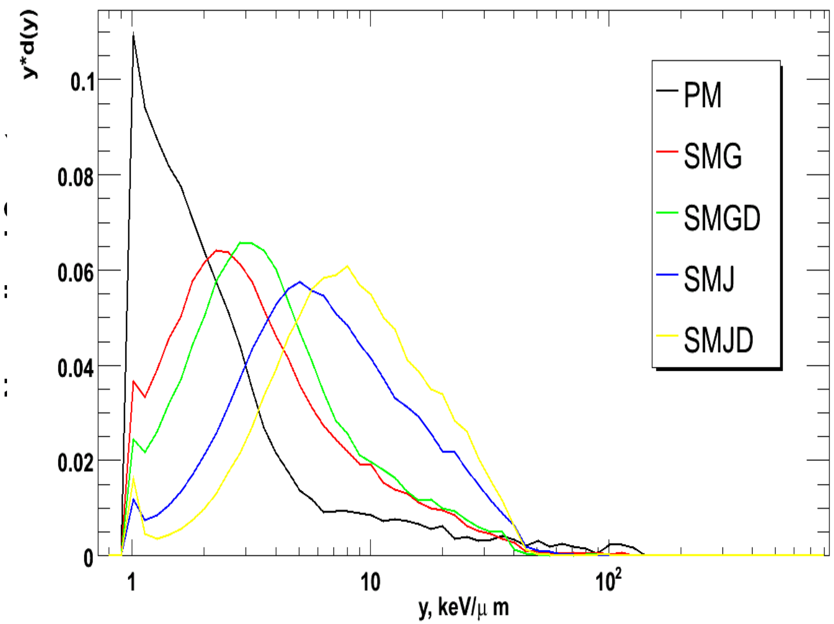

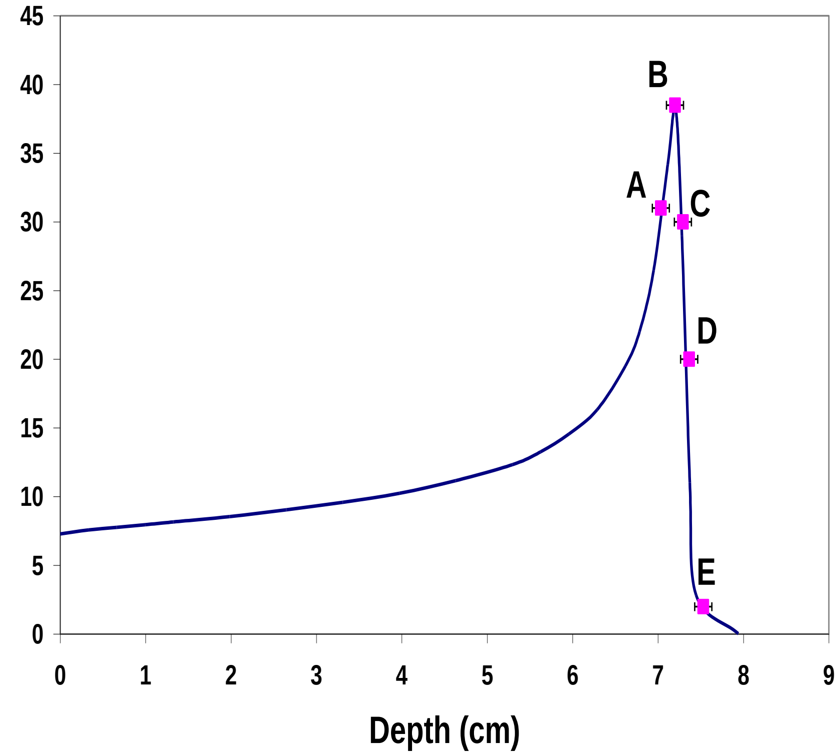

- Microdosimetric spectra from 10 mm SOI micro at consecutive positions in a Bragg Peak
- Possibility to estimate Q of the beam

For more details see: A Rosenfeld "Electronic Dosimetry in Radiotherapy", Rad. Meas., 41, 134-153, 2007

CENTRE FOR MEDICAL RADIATION PHYSICS
UNIVERSITY OF WOLLONGONG

Experimental Setup

- Prostate treatment conditions replicated
- The microdosimeter was moved laterally with respect to the field edge

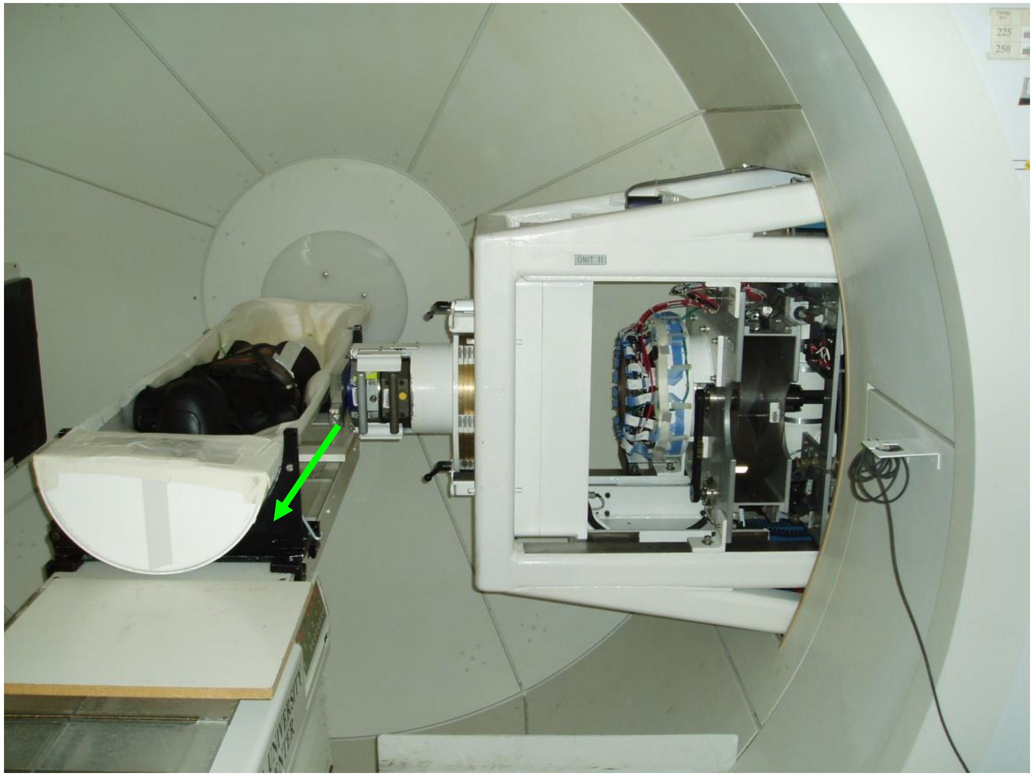

- Device centred to the height of the central axis
- Incident protons of 225MeV were utilised

Experimental Setup

- The microdosimeter was moved parallel to the central beam axis 5cm from the field edge.

- The device was centred to the height of the central axis

- Incident protons of 225MeV were used.

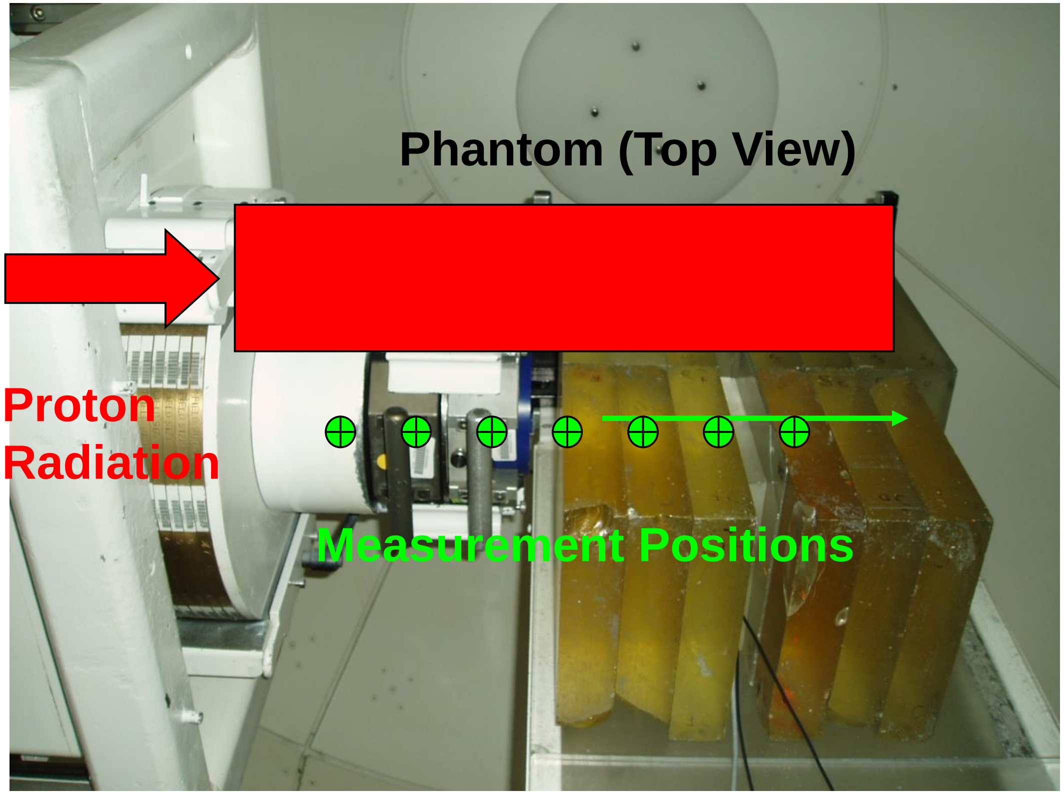

Proton Therapy- secondary cancer risk estimation

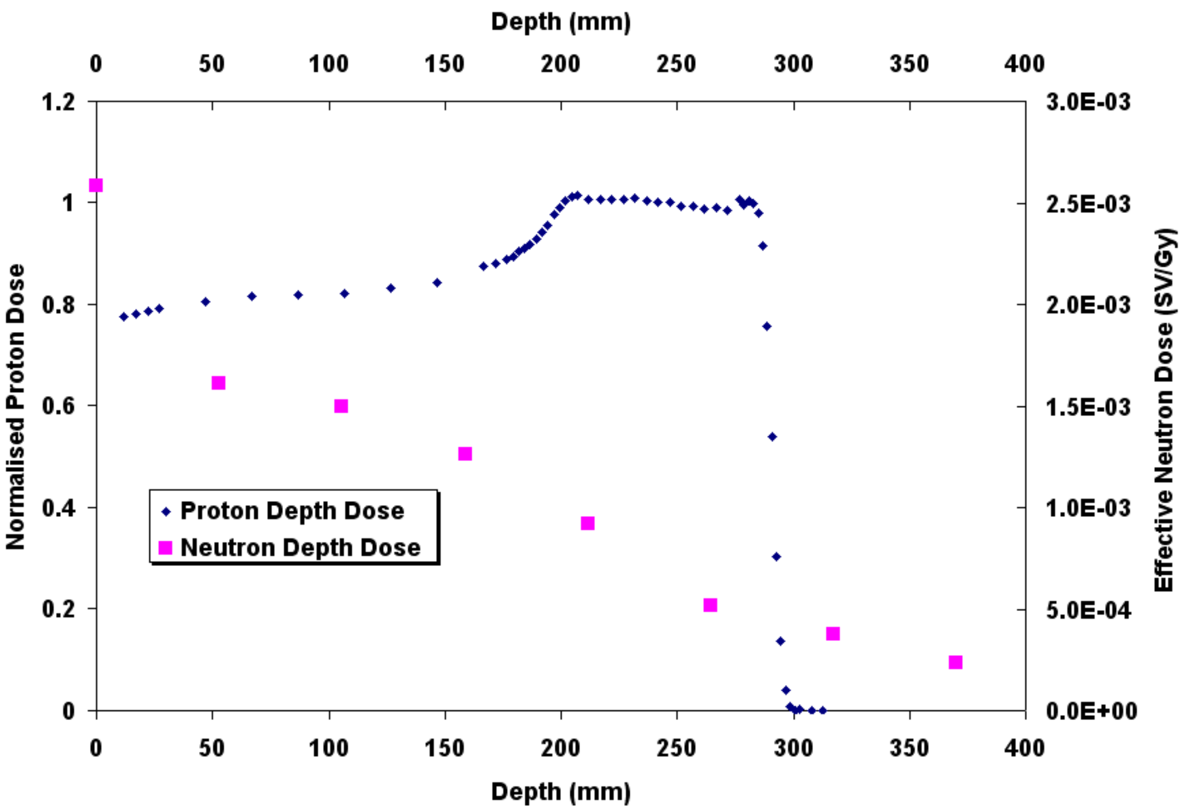

- Invited in phantom experiments were carried out at LLUMC and MGH proton therapy facilities
- All typical cancer treatment scenario with PT were investigated
- Measured dose equivalent was less then predicted that make confirmation of safety of PT

CMRP: Firstly measured dose equivalent with silicon SOI microdosimetry.

Results

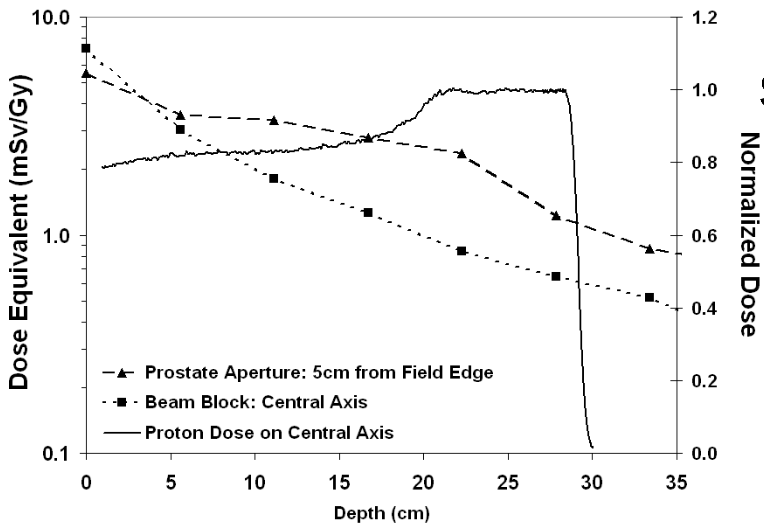

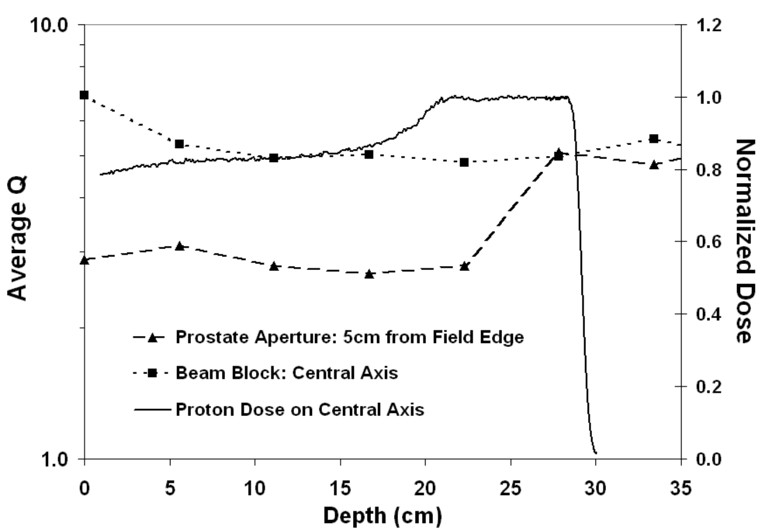

Scanning parallel to the beam at 5cm offset

- **0.9 mSv/Gy < $H_{aperture}$ < 5.5 mSv/Gy**
- **0.5 mSv/Gy < H_{block} < 7.1 mSv/Gy**
- **$H_{aperture}$ has a different dependence on depth than H_{block}**
- **Scattered primary protons affects H and the determination of Q up to 22.3 cm depth**
- **Downstream of the Bragg peak, difference in H is due to n generated in the phantom**

ΔE-E telescope: PBS vs Double Scattering

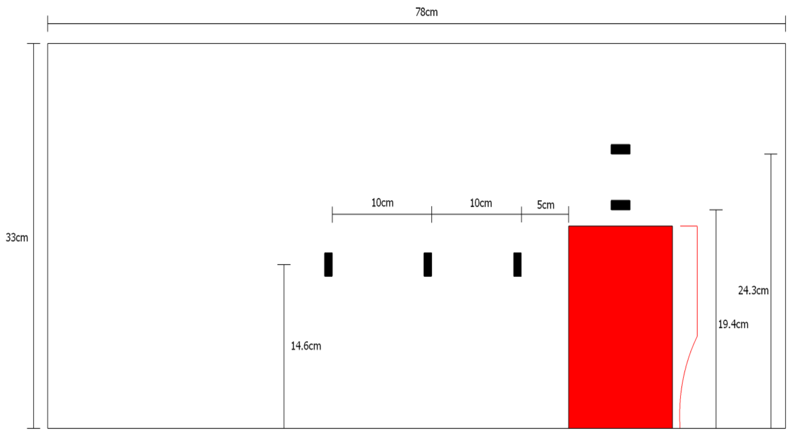

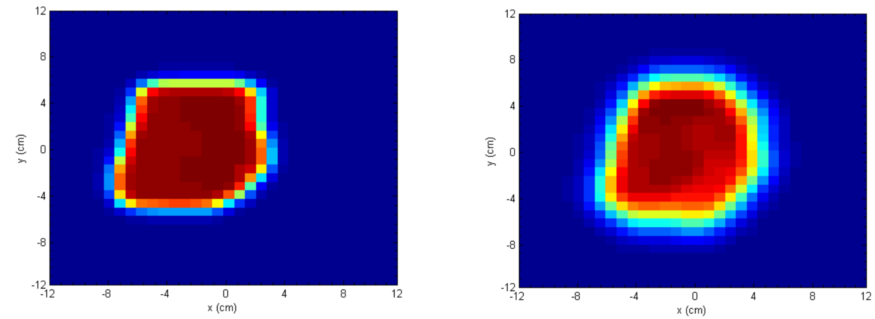

Beam shape for the double scattering (left) and pencil beam scanning (right) fields using the MatriXX detector (IBA dosimetry

The 5 measurement positions of the ΔE-E detector during the experiment.

ΔE-E spectra downstream of SOBP, on a the central axis:
(a) double scattering (b) pencil beam scanning

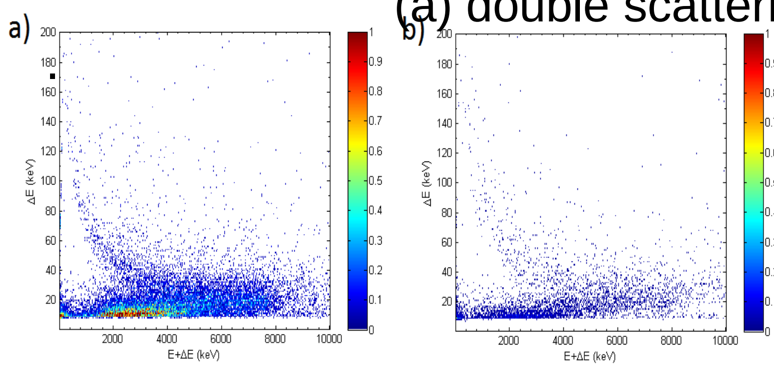

19.4cm depth

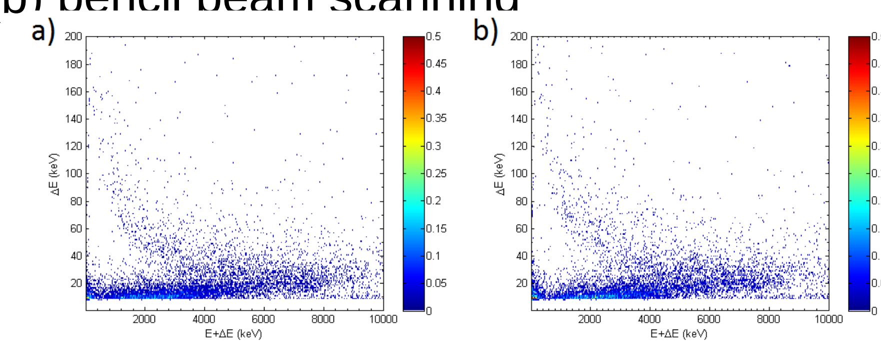

25 cm depth

Stephen Dowdell, PhD Thesis, CMRP UoW, May 2011
with B.Clasie, J.Flanz, A Fazzi, A.Pola ,S.Agosteo, A Rosenfeld

CENTRE FOR MEDICAL RADIATION PHYSICS | UNIVERSITY OF WOLLONGONG

ΔE-E telescope: PBS vs Double Scattering

ΔE-E spectra at a depth of 14.6cm in Lucite normalized counts/Gy in SOBP
(a) double scattering; (b).pencil beam scanning

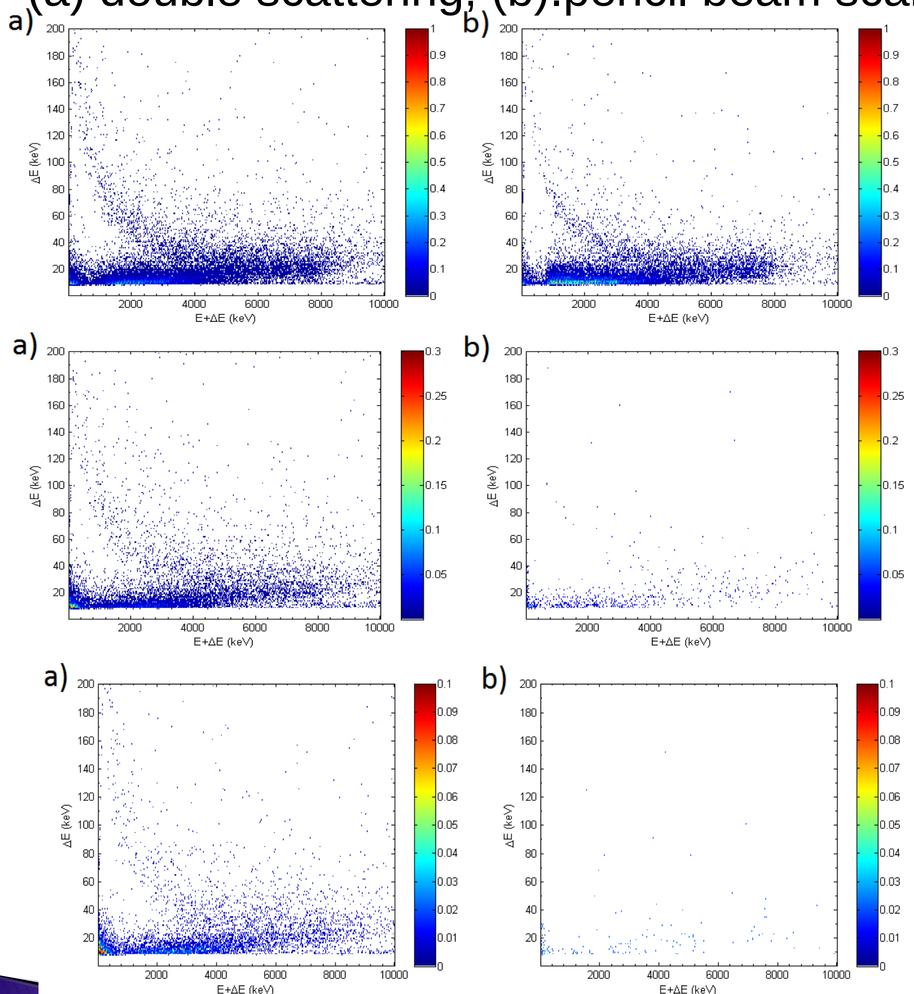

Lateral distance from the field edge

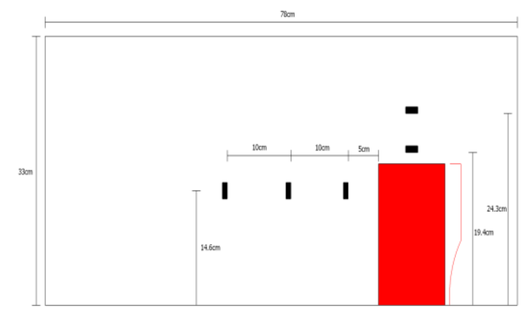

5 cm

15 cm

25 cm

- Direct confirmation of essential reduction of neutrons laterally out of field for PBS vs passive delivery
- Closer to the field contribution from scattered protons for PSB higher due to larger penumbra in comparison with passive delivery

X-ray Medical LINAC

Photoneutron Production (γ,n) reactions

Component	15 MeV	18 MeV	20 MeV
Target	9 % (W,Cu)	16 % (W,Cu)	17.2% (W,Cu)
Primary Colimator	38% (W)	41% (W)	36% (W)
Flattening Filter	22% (W)	9% (Fe,Ta)	10.4% (Fe,Ta)
Jaws	29% (W)	35% (W)	36% (W)
Other (shielding, etc)	1.20%	1.40%	1%

Table 1: Monte Carlo calculation of the % of photo-neutron production

in various linac component's for a Varian 2100/2300C Linac. [1, Mao]

Maximum Photon Energy (MeV)	Average Neutron Energy (MeV)
15	1.15
18	1.25
20	1.31
25	1.46

Table 2: Average photo-neutron energies for high-energy Linacs. [2, Facure]

Figure 1: Varian 18MV Medical Linac cross sectional view. [3]

Photo-Neutron Energy Spectrum in a Radiotherapy Treatment room

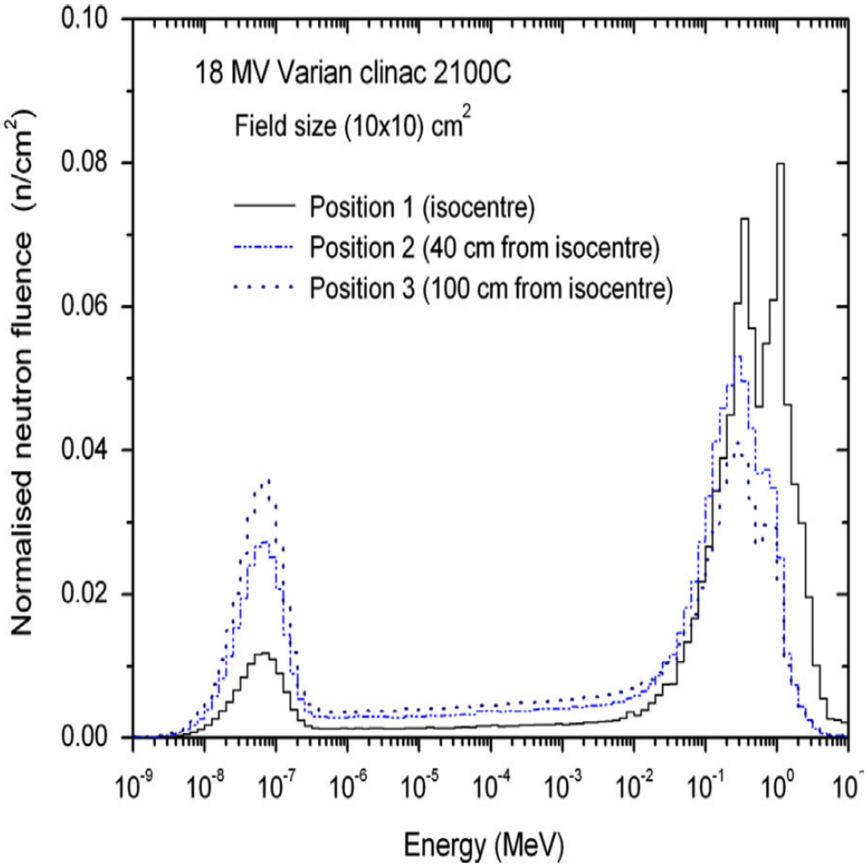

Figure 2: Photo-neutron Spectra at the Patient Couch, as measured using CR39 track detectors. [4, Alem]

Evaporation neutrons constitute the greatest part of the photo-neutrons and their spectra, as described by Tosi et al [5]:

$$\frac{\mathrm{d}N}{\mathrm{d}E_\mathrm{n}} = \frac{E_\mathrm{n}}{T^2}\exp\left(\frac{-E_\mathrm{n}}{T}\right)$$

$$n(E) = A\frac{E}{T^2}Exp\left[-\frac{E}{T}\right] + B\frac{ln\left[\frac{E_{max}}{E+S}\right]}{\int_0^{E_{max}-S} ln\left[\frac{E_{max}}{E+S}\right]dE}$$

Evaporation neutrons

Fast neutrons

Single Event Upset of Static random access memory (SRAM)

(SEU) in digital devices are produced by the ionization charge released from the interaction in silicon of particles like heavy ions, recoil nuclei or nuclear fragments from neutron interactions.

SRAMs change the logical level of their cells when are exposed to neutrons.

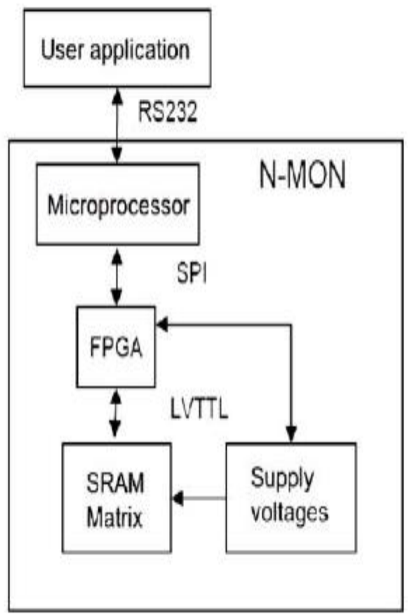

Figure 6: SRAM readout board. [Auerlio, 10]

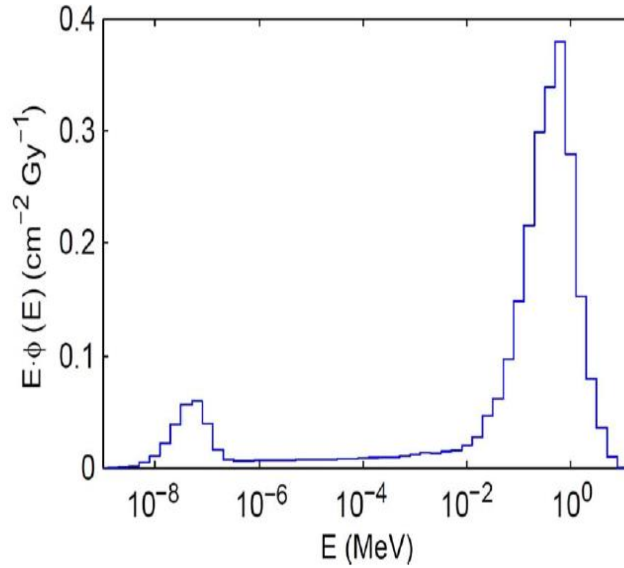

Figure 7: Neutron lethargy for a medical linac working at 15MV measured using SRAM device. Fluence normalized to 1 Gy photon Dose. [Auerlio, 10]

3D Thin Neutron Detector – 10um

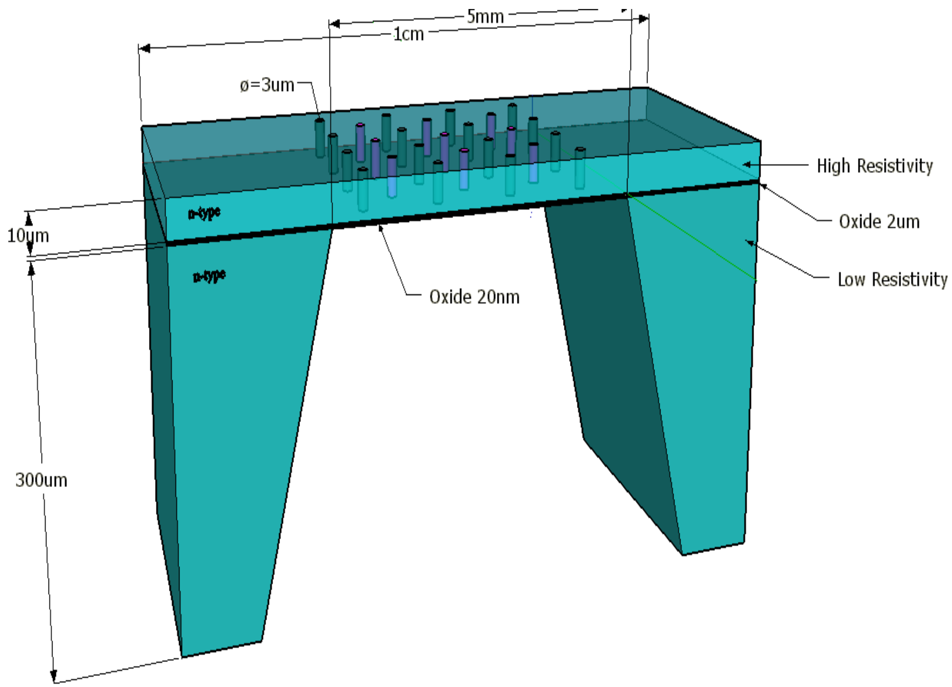

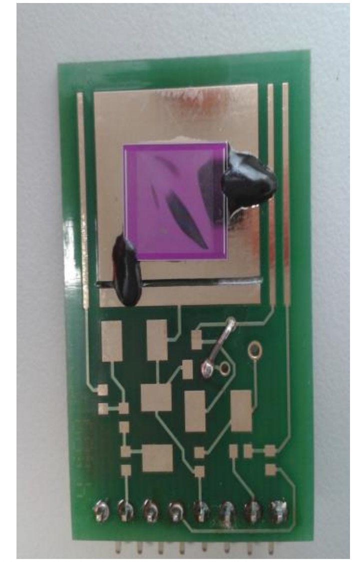

- CNM: Spanish Detector
- n -type silicon
- High gamma rejection
- Fast response

(8b)

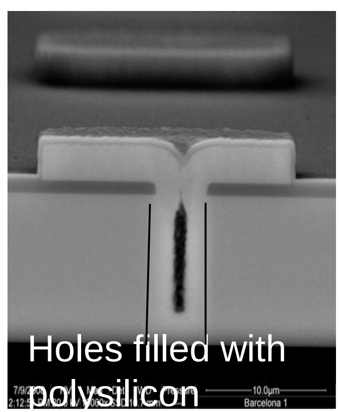

(8c)

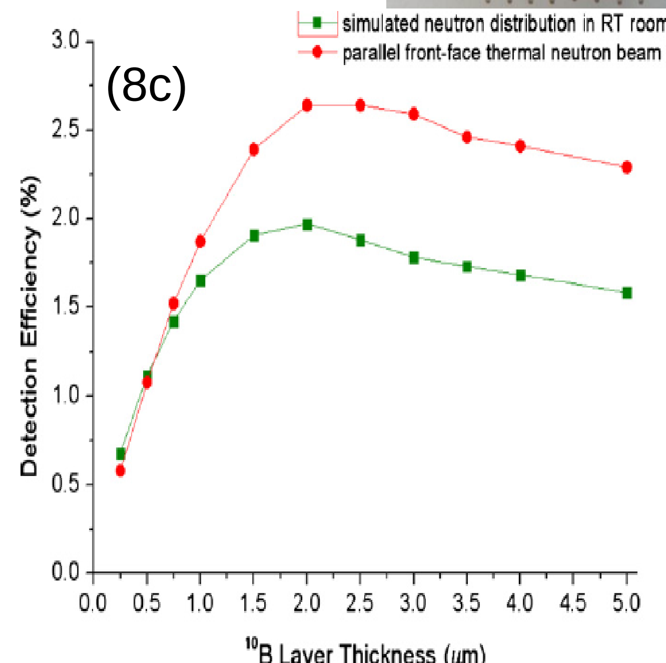

Figure 8c:

Figure 8a, 8b: 3D thin Neutron Detector Schematic.

[CNM, 11]

Neutron Measurements in RT Room with Ultra thin Detectors adapted with

$$^{10}\mathrm{B} + n \xrightarrow{94\%} \alpha\,(1.47\,\mathrm{MeV}) + {}^{7}\mathrm{Li}\,(0.84\,\mathrm{MeV}) + \gamma\,(0.48\,\mathrm{MeV})$$

$$\xrightarrow{6\%} \alpha\,(1.78\,\mathrm{MeV}) + {}^{7}\mathrm{Li}\,(1.01\,\mathrm{MeV})$$

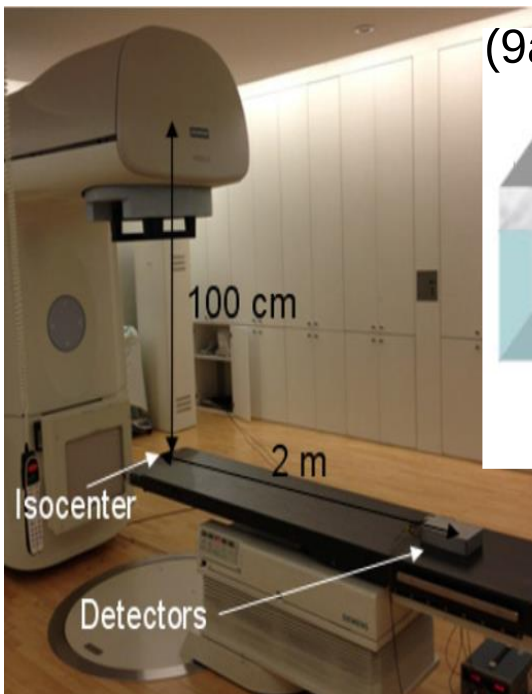

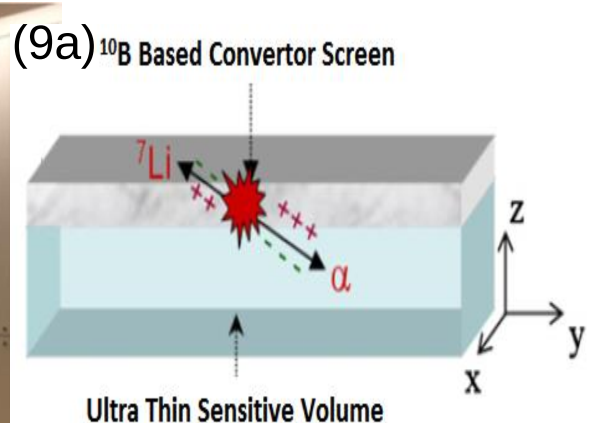

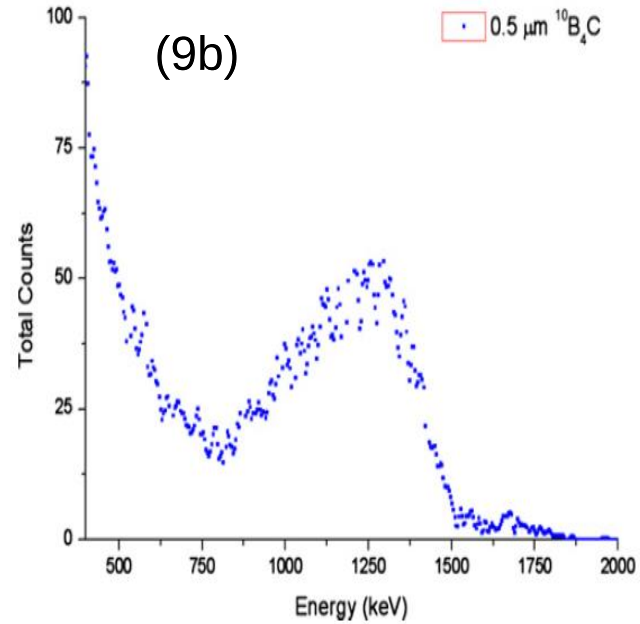

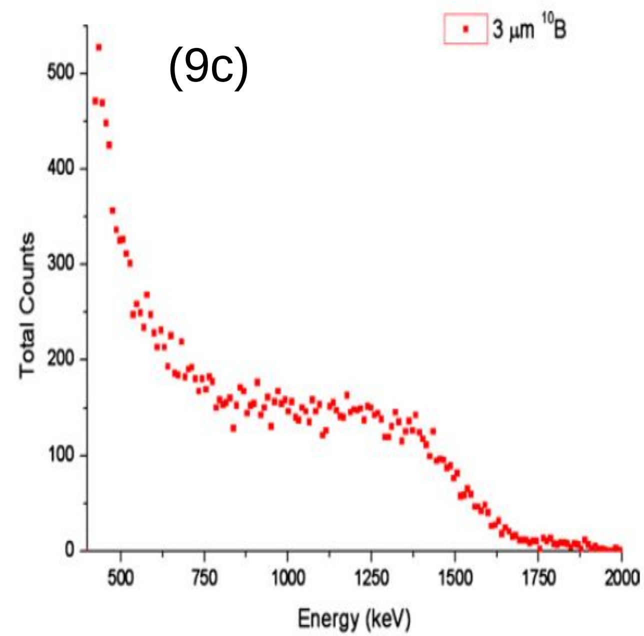

- 10x10 Field Size
- 1000 MU at 500MU/min

Figure 9a, 9b, 9c : 3D thin Neutron Detector Schematics.

[12]

Acknowledgement

- Dr Mark Yudelev for pleasant collaborations in FNT at Gershenson Cancer Centre , Detroit and some slides sharing
- Dr Marco Petasecca for RD slides sharing
- Prof Toru Kobayashi , KURR for collaboration on BNCT and some slides sharing

Vanja Grakanin PhD student for help in some slides preparation related to LINAC.

All CMRP colleagues involved on presented research

MMND & ITRO 2016

Mini-Micro-Nano-Dosimetry and
Innovative Technologies in Radiation Oncology Workshops